Physics and Observations of Extragalactic Jets

Lukasz Stawarz

KIPAC, Stanford University, USA

Extragalactic Jets

10^{22}-10^{24} [cm]

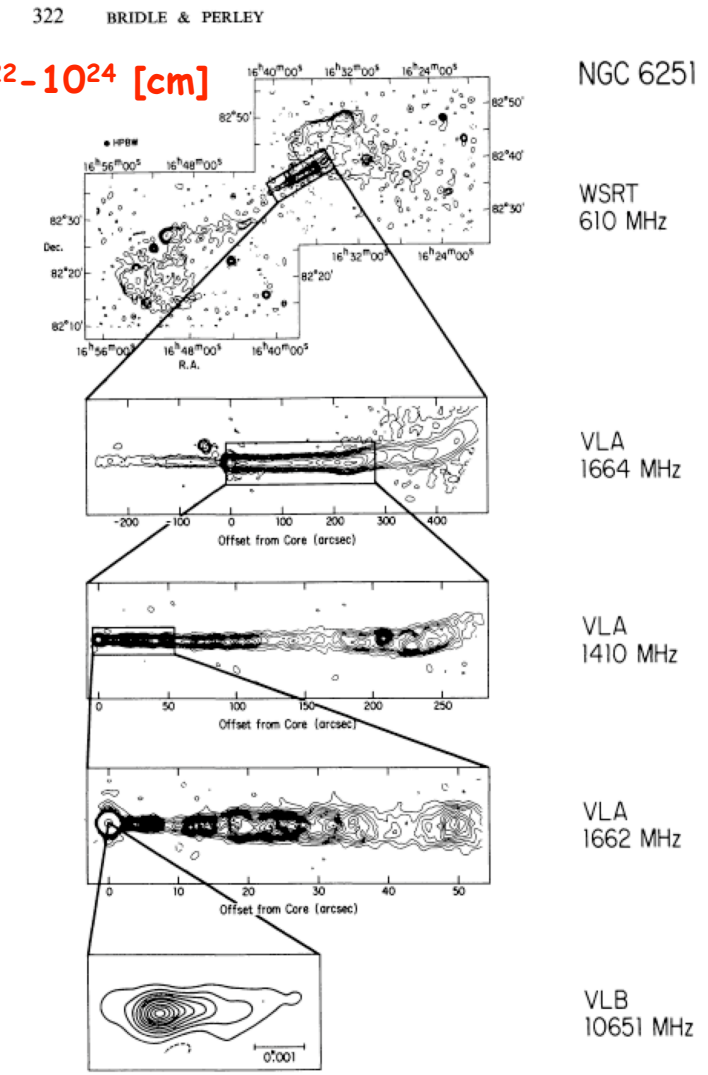

10^{16}-10^{17} [cm]

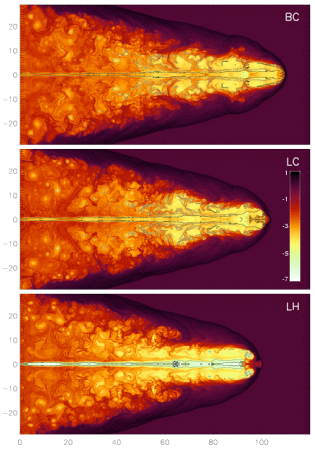

Rj ~ 10^{21}-10^{24} [cm]
MHD/HD
(Scheck+ 2002)

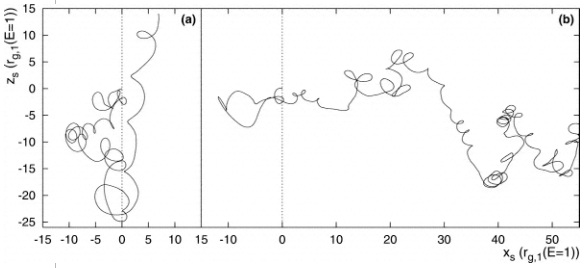

$r_g \sim E_e/eB \sim 10^{16}$ $(\gamma/10^8)$ $(B/10^{-5}G)^{-1}$ [cm]
MC
(Niemiec & Ostrowski 2004)

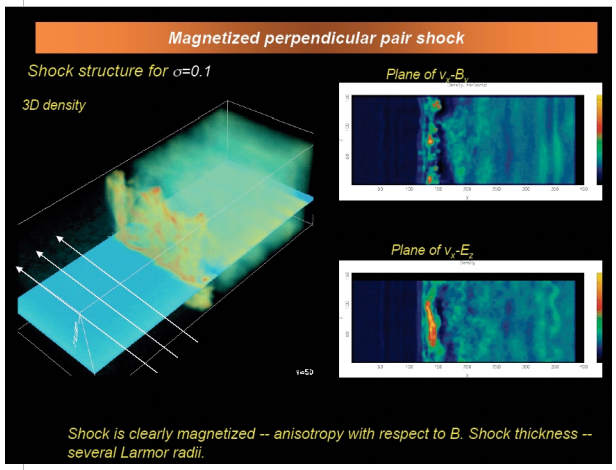

$\lambda_e \sim c/\omega_e \sim 10^9$ $(n_e/10^{-5}cm^{-3})^{-1/2}$ [cm]
PIC
(Spitkovsky 2005)

A Role of the Jet Magnetic Field

Magnetic field (MF) assures fluid-like character of the jet plasma and is a source of a fluid viscosity.

$$\langle v_{\rm e}\rangle \approx \left(\frac{kT}{m_{\rm e}}\right)^{1/2}$$

mean velocity of thermal electrons

$$\lambda_{\rm C} = \frac{\langle v_{\rm e}\rangle}{\omega_{\rm col}} \quad \text{where} \quad \omega_{\rm col}^{ee} = \frac{2\pi e^4 n_{\rm pl}\ln\Lambda}{m_{\rm e}^2\,(3kT/m_{\rm e})^{3/2}} \approx \sqrt{\frac{m_{\rm p}}{m_{\rm e}}}\,\omega_{\rm col}^{pp} \approx \frac{m_{\rm p}}{m_{\rm e}}\,\omega_{\rm col}^{ep}$$

Coulomb mean free path

$$r_{\rm L} = \frac{\langle v_{\rm e}\rangle}{\omega_{\rm L}^e} \quad \text{where} \quad \omega_{\rm L}^e = \frac{eB}{m_{\rm e}c}$$

electron gyroradius

$$\lambda_{\rm D} = \frac{\langle v_{\rm e}\rangle}{\omega_{\rm pl}^e} \quad \text{where} \quad \omega_{\rm pl}^e = \left(\frac{4\pi e^2 n_{\rm pl}}{m_{\rm e}}\right)^{1/2}$$

Debye screening length

$$\lambda_{\rm C} \gg \ell \gg \lambda_{\rm D},\, r_{\rm L}$$

Extragalactic Jets:
magnetized, collisionless, and neutral fluids

Ideal (NR) MHD

$$\frac{\partial}{\partial t}\vec{B} = \vec{\nabla} \times \left(\vec{v} \times \vec{B}\right)$$

$$\frac{\partial}{\partial t}\rho + \vec{\nabla}(\rho\vec{v}) = 0$$

$$\left(\frac{\partial}{\partial t} + \vec{v}\cdot\vec{\nabla}\right)\left(\frac{p}{\rho^{\hat{\gamma}}}\right) = 0$$

$$\rho\left(\frac{\partial}{\partial t} + \vec{v}\cdot\vec{\nabla}\right)\vec{v} = -\vec{\nabla}p + \frac{1}{4\pi}\left(\vec{\nabla}\times\vec{B}\right)\times\vec{B}$$

$(j_M \times B) / c$

Perfect conductivity limit (negligible resistivity ~ high magnetic Reynold number)

$\eta \to 0$ (or $R_M \gg 1$)

➔ $E = -\beta \times B$

Electric field (EF) vanishes in the plasma rest frame. MF is advected with the plasma so that the magnetic flux is conserved (`flux freezing').

Non-relativistic Force-Free:

$\beta_M \ll 1$ and $\sigma \gg 1$

MF is in equilibrium with itself (balance between MF pressure and tension forces). Currents flow parallel to the field lines.

$$\sigma \equiv \frac{v_{\rm A}^2}{v^2} = \frac{U_{\rm B}}{U_{\rm kin}} = \frac{B^2}{4\pi\rho v^2}$$

$$\beta_{\rm M} \equiv \frac{p}{U_{\rm B}} = \frac{8\pi p}{B^2}$$

$$\vec{j}\times\vec{B} = 0$$

Supermassive Black Holes

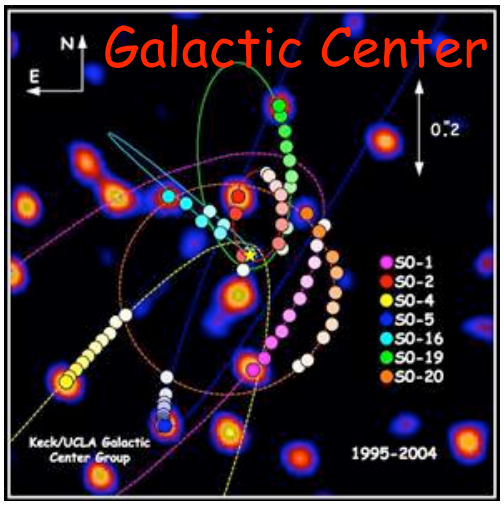

"No Hair" theorem: BH is characterized solely by its mass M and angular momentum J (**Kerr 63**; no electric charge assumed), no matter on the history of the formation process. Thus, BH cannot have its own MF. However, BH can be merged into an external MF supported by external currents. The maximum energy density of such field (B_E) is therefore equal to the energy density of the matter accreting at the Eddington rate (L_E).
[e.g., **Rees 84**, **Begelman 02** and ref. therein]

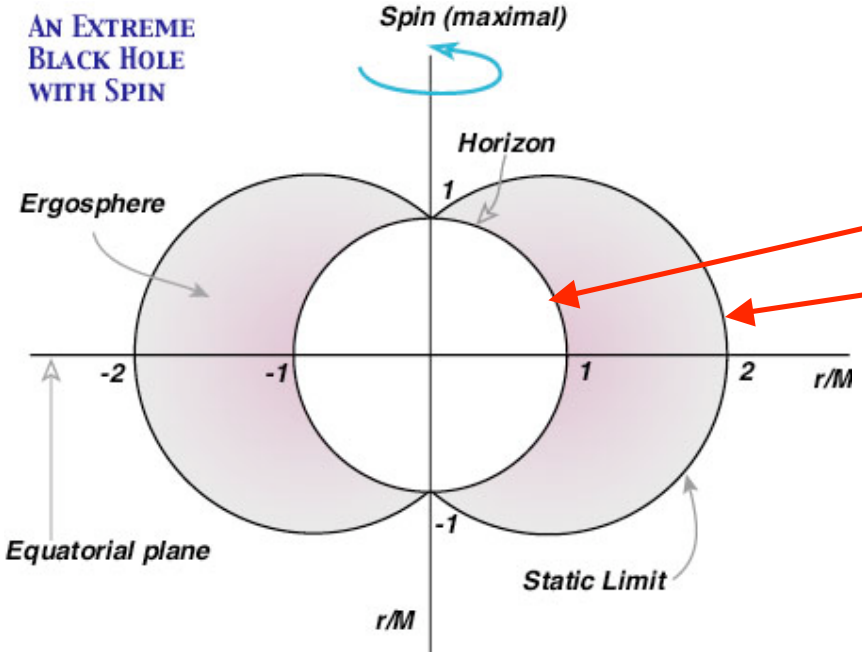

$$r_{\rm g} = \frac{GM}{c^2} \approx 10^{13} M_8\,[{\rm cm}] \quad \text{where} \quad M_8 \equiv \frac{M}{10^8 M_\odot}$$

$$a = \frac{J}{Mc} \quad \text{and} \quad a_{\rm max} = r_{\rm g}$$

$$r_{\rm S} = r_{\rm g} + \sqrt{r_{\rm g}^2 - a^2} \quad , \quad r_{\rm C} = r_{\rm g} + \sqrt{r_{\rm g}^2 - a^2 \cos^2\theta}$$

$$\Omega_{\rm S} = \left(\frac{J}{J_{\rm max}}\right) \frac{c}{2r_{\rm S}}$$

$$L_{\rm E} = \frac{4\pi G M m_{\rm p} c}{\sigma_{\rm T}} \approx 10^{46} M_8\,[{\rm erg/s}]$$

$$B_{\rm E} = \left(\frac{2L_{\rm E}}{r_{\rm g}^2 c}\right)^{1/2} \approx 6 \times 10^4 M_8^{-1/2}\,[{\rm G}]\,.$$

How Much Power Is Available?

BH embedded in a uniform MF acquires a quadrupole distribution of the electric charges with the corresponding poloidal electric field (**Wald 74, Phinney 83**). Thus, power can be extracted by allowing currents to flow between the equator and poles of a spinning BH within the magnetosphere above the event horizon ("unipolar inductor"). For the conserved magnetic flux and $B \sim B_E$, the Faraday and Gauss laws imply the potential drop (electromotive force) involved

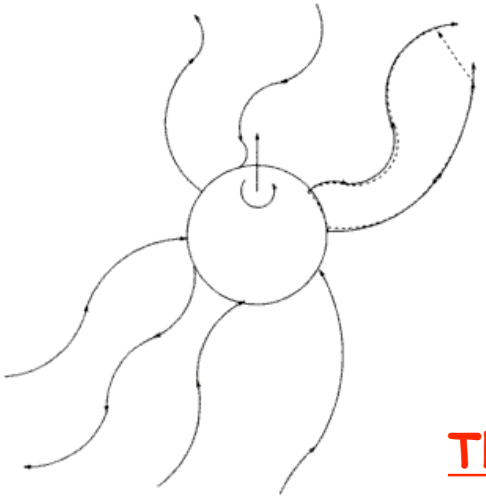

$$\Delta V \equiv -\oint \vec{E}\cdot d\vec{l} = \oint \left(\frac{\vec{v}}{c}\times\vec{B}\right)\cdot d\vec{l} \sim \frac{J\,B\,r_{\rm g}}{J_{\rm max}} \sim 10^{18} M_8^{1/2}\frac{J}{J_{\rm max}}\,[{\rm cgs}]$$

$$E_{\rm max} \sim e\,\Delta V \sim 3\times 10^{20} M_8^{1/2}\frac{J}{J_{\rm max}}\,[{\rm eV}]$$ *UHECRs!*

(emf results from different velocties of ZAMOs at different distances from BH)

This gives the maximum power that can be extracted:

$$P \sim \Delta V\cdot I \sim \frac{\Delta V^2}{\Re} \sim \frac{c}{4\pi}\left(\frac{J}{J_{\rm max}}\right)^2 B^2 r_{\rm g}^2 \sim 10^{45}\, M_8 \left(\frac{J}{J_{\rm max}}\right)^2\,[{\rm erg/s}]$$

(The event horizon of BH behaves like a spinning conductor with finite conductivity. Hence $D_M \sim r_g c$, since MF has to decay just like its supporting currents flowing into the event horizon on the dynamical timescale $\sim r_g/c$. This gives the BH resistance $\Re \sim 4\pi/c$.)

How To Extract This Power?

Blandford & Znajek 77: with a force-free magnetosphere added to a rotating BH embedded in an external MF, electromagnetic currents are driven, and the energy is released in the expense of the BH rotational energy ("reducible mass")

$E_{rot}(a=r_g) \sim 0.3\ M\ c^2 \sim 5 \times 10^{61}\ M_8$ **[erg]** (pdV ~ 10^{62} ergs required in clusters)

*[scenario inspired by earlier developed models for young stars (**Weber & Davis 67**), pulsars (**Michel 69**, **Goldreich & Julian 70**), and accretion disks in active galaxies (**Blandford 76**, **Lovelace 76**, **Bisnovatyi-Kogan & Ruzmaikin 76**)]*

i) MF is dragged from outer distances and amplified by the accreting matter. It is assumed to be initially poloidal, aligned to the BH spin, supported by the toroidal currents within the accretion disk, with the intensity $B \sim B_E$ close to the event horizon.

ii) Due to the frame-dragging effect, MF in the ergosphere is forced to rotate with the angular velocity $\varpi \sim \Omega_S\ (r_S / r)^3$ as measured by ZAMO. Quadrupole poloidal EF is thus induced (in every frame) in the vacuum above the BH surface.

iii) This vacuum is unstable for the pair creation. The created pairs accelerated by the aligned EF initiate electromagnetic cascades (curvature, synchrotron, and IC emission). In this way the force-free magnetosphere is established.

iv) Charge distribution formed in the magnetosphere supports poloidal EF, and the generated currents create the additional poloidal and toroidal MF components.

v) The combination of the poloidal EF and the toroidal MF leads to the radial Poynting flux which carry away energy. The combination of the poloidal EF and MF carries away angular momentum of the Kerr BH.

BH-Torus Simulations

Hawley, Krolik, De Villiers, Hirose: 3D non-conservative GR ideal MHD simulations of a long-term (~10^4 r_g) evolution of an isolated gaseous torus orbiting rapidly ($a/r_g > 0.9$) rotating BH with no initial large-scale magnetic field; BL coordinates.

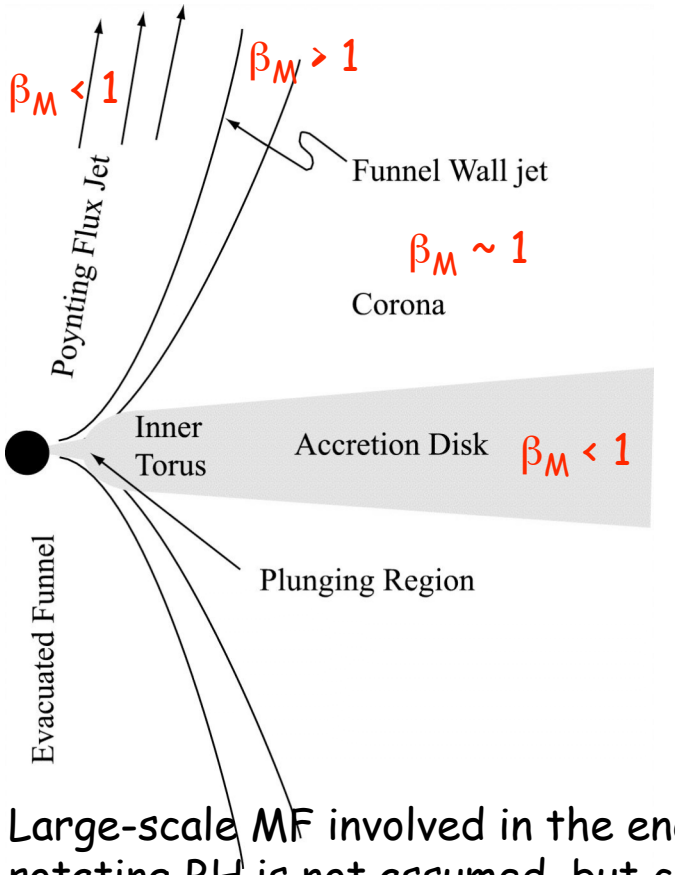

Hawley & Krolik 06: The torus is initially supported against the gravity by pressure and rotation, and the polar regions above the BH are initially empty due to centrifugal forces and no initial MF assumed. Small loops of a weak poloidal MF added at the beginning to the torus ($\beta_M \sim 100$), which then becomes unstable for MRI and thus turbulent. The small-scale MF starts to be then amplified (forming large scale poloidal MF component), angular momentum starts to be transported, and the accretion begins through the "plunging region". Above the surface of the disk, a hot corona ($\beta_M \sim 1$) is immediately established.

Large-scale MF involved in the energy extraction from rotating BH is not assumed, but created self-consistently by the accreting matter. The power of the outflow relative to the accretion rate (as well as a relative strength of the central and funnel jets) is a strong function of the BH spin.

TWO-COMPONENT JET:
In the polar regions, Poynting-flux dominated outflow emanating from the ergosphere is observed ("BZ jet"). It is surrounded by the matter-dominated funnel jet. Both ouflows are collimated by the torus and corona pressures.

EM Jets

McKinney, Gammie: axisymmetric conservative GR ideal MHD simulations of a long-term (~10^4 r_g) evolution of an isolated gaseous torus orbiting rapidly ($a/r_g > 0.9$) rotating BH with no initial large-scale magnetic field; modified KS coordinates.

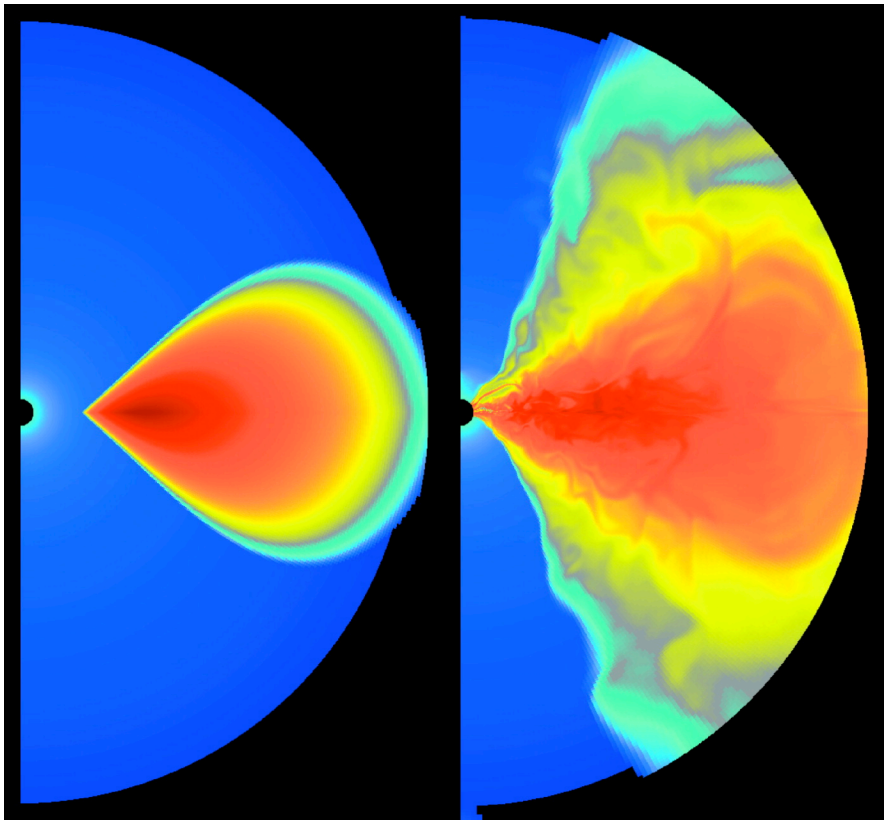

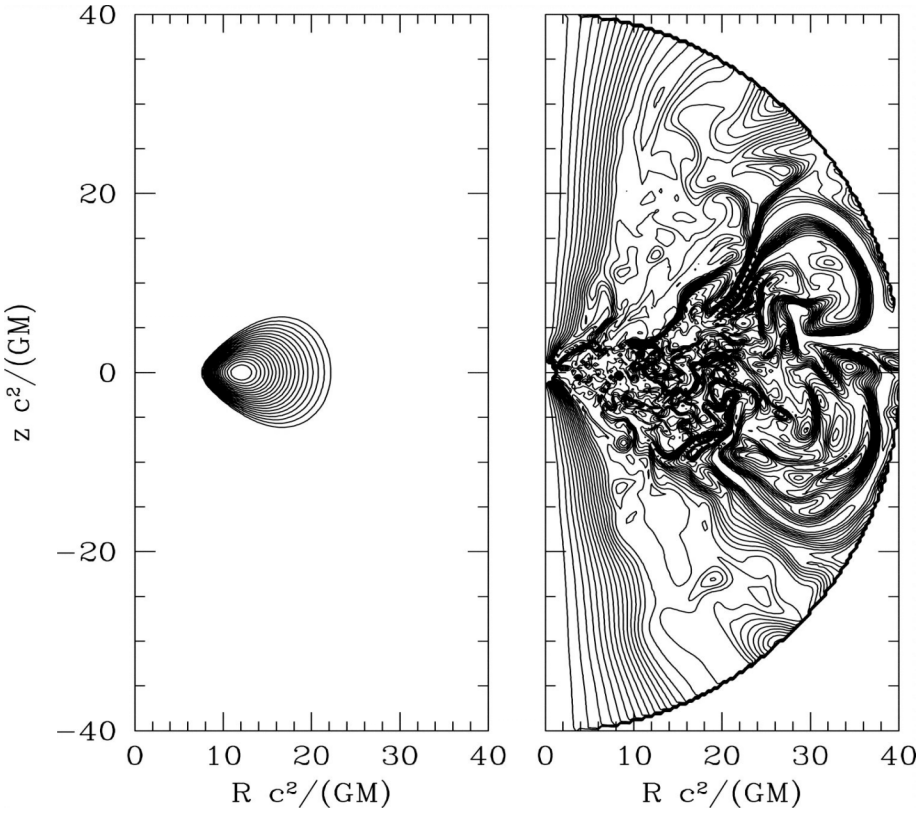

McKinney & Gammie 04 (rest density indicated by colors; poloidal magnetic field indicated by contours): results very similar to those obtained by Hawley et al. In particular, a two-component outflow with a force-free relativistic (v~c) spine and a matter-dominated slow (v ~ 0.75 c) outer sheath/wind is observed. Little mixing between these two components noted.

Disk Outflows

Open poloidal MF lines that leave the surface of a heavy thin accretion disk and extend to large distances can extract the energy and angular momentum of the accreting matter.

$$\Phi_{\rm cg} \equiv \Phi_{\rm grav} - \frac{1}{2}\Omega^2 r^2 = -\frac{GM}{r_0}\left[\frac{1}{2}\left(\frac{r}{r_0}\right)^2 + \frac{r_0}{\sqrt{r^2+z^2}}\right]$$

The centrifugal-gravitational potential is decreasing along the MF lines inclined <60deg to the disk surface (for Newtonian gravity and Keplerian rotation; **Blandford & Payne 82**).

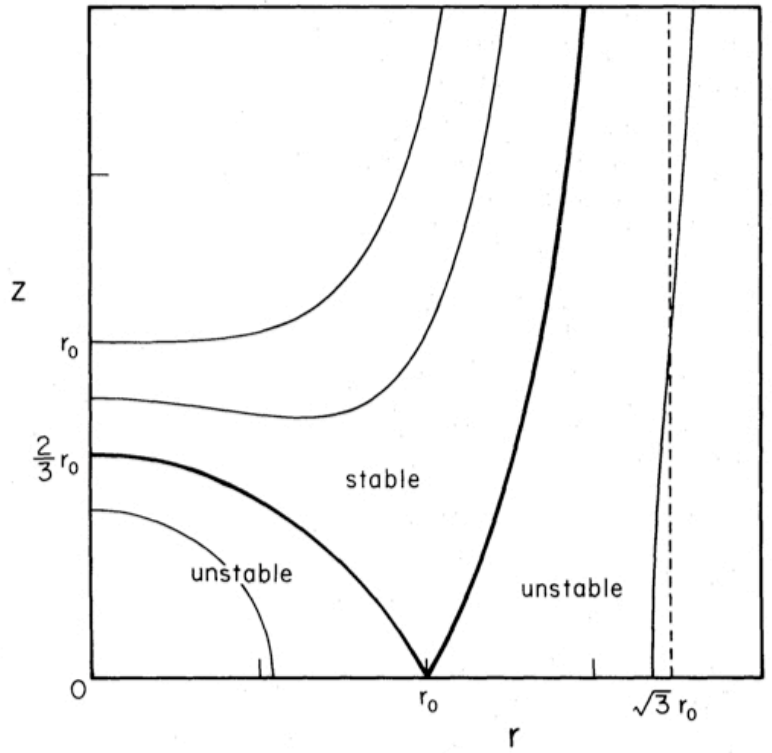

Dynamically dominating matter within the disk forces the frozen-in open poloidal MF lines to rotate, say, at the local Keplerian angular velocity $\Omega = (GM/r_0^3)^{1/2}$, where r_0 is the radius of a footpoint for a given line. Since charged particles (both protons and electron-positron pairs) can easily leave the accretion flow, one should expect a low-density magnetosphere to be generated above the disk surface.

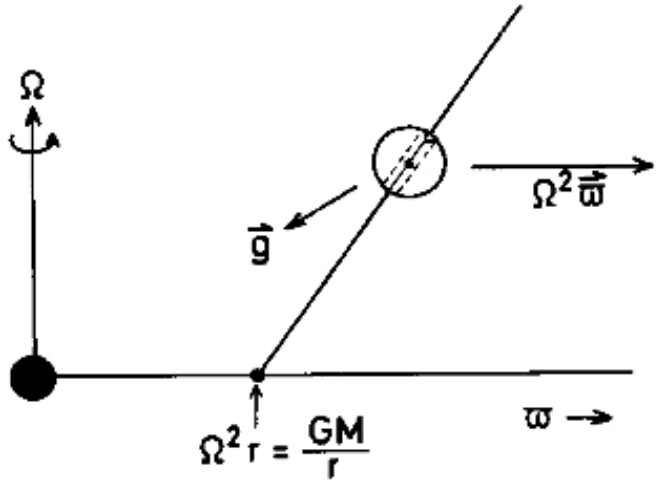

Alfven Surface

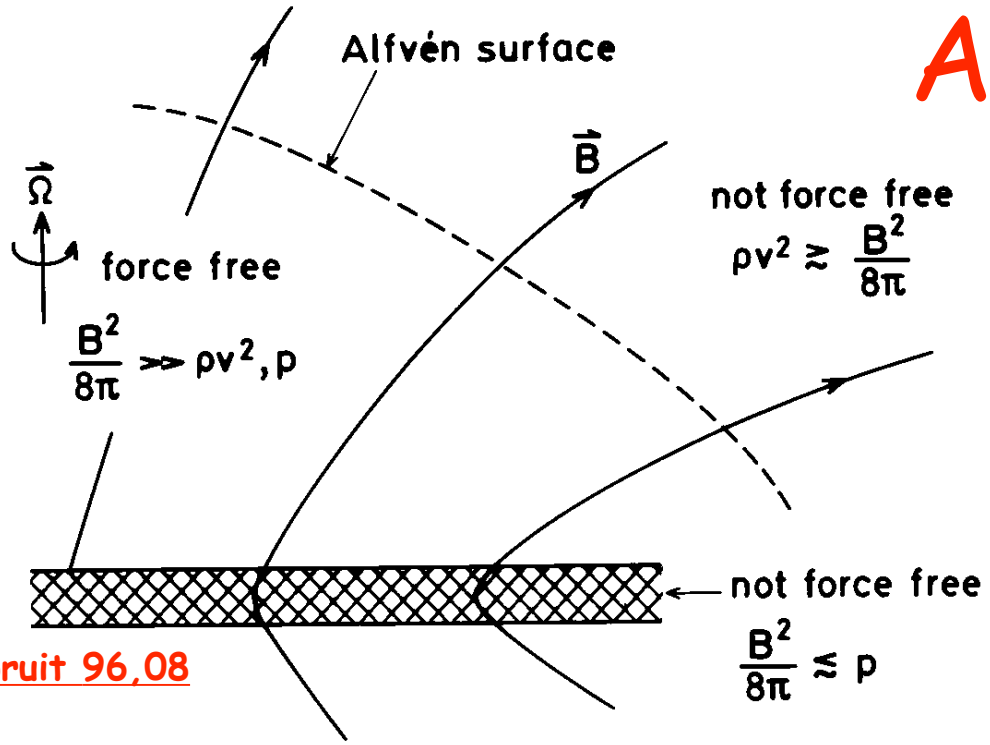

Spruit 96,08

Michel's magnetization parameter (essentially the ratio of Poynting and inertial fluxes):

$$\sigma_{\rm M} \equiv \frac{\phi_{\rm M}^2 \Omega^2}{4\dot{m}c^3} = \left(\frac{v_{\rm A}^P}{c}\right)^2 \left(\frac{r}{R_{\rm L}}\right)^2 \left(\frac{v_{\rm P}}{c}\right)^{-1}$$

where $\phi_{\rm M} = B_P r^2$ is the poloidal magnetic flux, $\dot{m} = \pi \rho v_P r^2$ is the mass flow rate, and $\Omega = c/R_{\rm L}$.

The open MF lines purely poloidal initial configuration are forced to co-rotate with the high-β_M disk, while the matter is centrifugally driven outward into the low-β_M corona and moves along the open field lines. When the velocity of the fluid approaches the poloidal Alfven velocity, $v_P = v_{A,P} \equiv B_P/(4\pi\rho)^{1/2}$ (i.e., near the Alfven surface R_A), the matter cannot be accelerated by the centrifugal forces anymore. Note that the relativistic velocities at the Alfven surface can be reached only if the Alfven speed is relativistic itself, i.e. if the magnetospheric plasma is highly magnetized, and the Alfven radius approaches the light cylinder $R_L = c/\Omega$. Note also that the force-free approximation, which may be valid in between the disk and the Alfven surfaces, is obviously violated around and beyond the later critical surface.

Beyond Alfven Surface

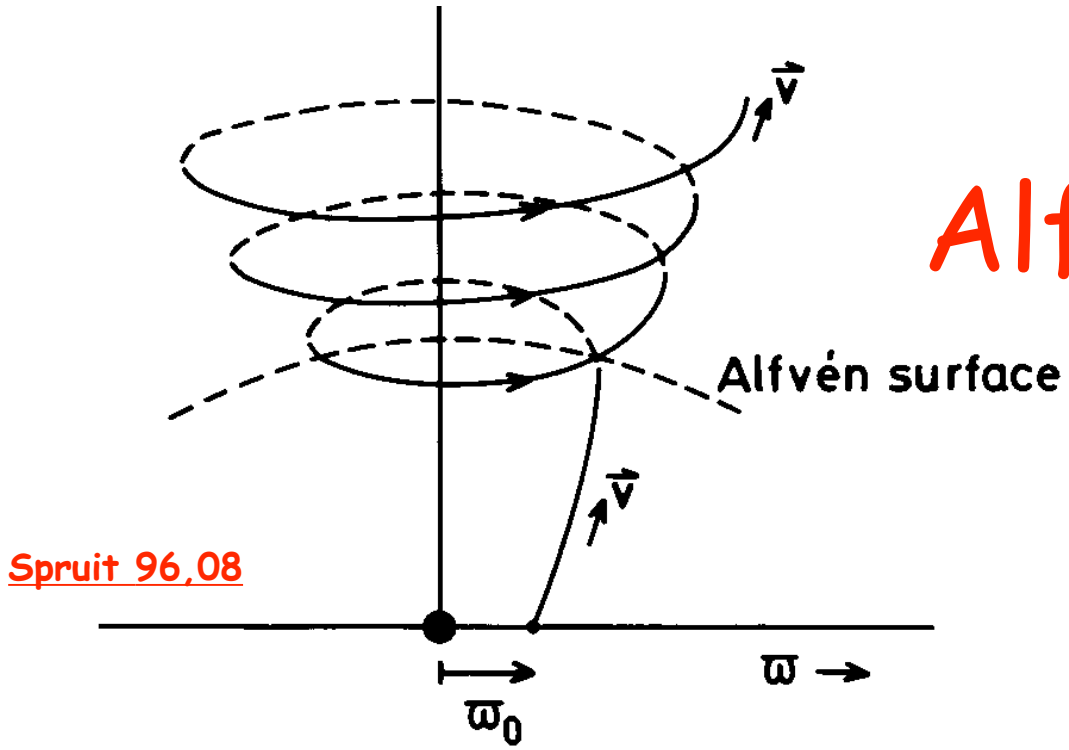

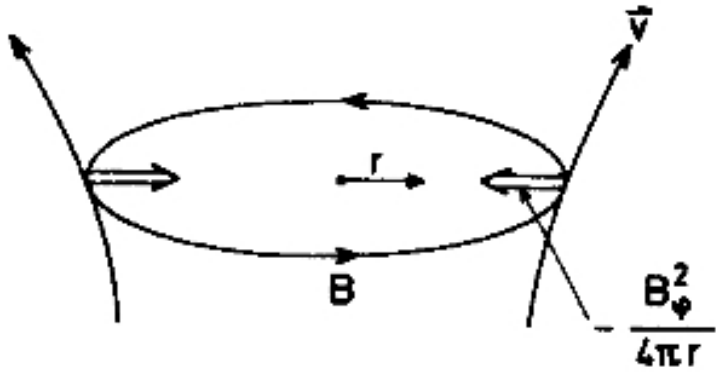

Beyond the Alfven surface the poloidal MF is not strong enough to enforce the co-rotation. Instead, inertia of the matter becomes important, and the gas starts to wind up the MF lines, forming the spiral shape beyond the Alfven surface. Such toroidal MF created by the backward twisting of the rotating poloidal component becomes dominant at further radii (relatively close to the Alfven surface, however) near the rotation axis. Note that by virtue of the Ampere's law, this configuration carries a poloidal current. Meanwhile, the curvature force of the toroidal field collimate the outflow by compressing the outflowing matter toward the jet axis (`hoop stresses') due to the $\mathbf{j}\times\mathbf{B}_T$ force (note that the currents flow along the magnetic surfaces). Such collimation induces a reduction in the poloidal MF flux along the poloidal streamlines, i.e. a reduction of the Poynting flux along the flow. Because of this, the gradient of the MF pressure associated with the toroidal field drives further acceleration of the outflow beyond the Alfven surface up to the fast magnetosonic surface R_F (where $v_P = v_{A,tot} \equiv B_{tot}/(4\pi\rho)^{1/2}$), increasing the plasma kinetic energy along the jet.

KH and CD Instabilities

- Jets are subjected to Kelvin-Helmholtz (KH) instabilities, for which the source is a relative kinetic energy between the outflow and the ambient medium. Relativistic velocities and longitudinal MF (if strong enough) may stabilize an outflow (**Birkinshaw 91, Hardee 07, Perucho+07**).
- Magnetized jets collimated by toroidal MF are also subjected to current-driven (CD) Z-pinch instabilities. These may re-arrange MF configuration, leading to disruption of an outflow and enhanced energy dissipation (**Appl & Camenzind 92, Eichler 93, Spruit+97, Begelman 98, Lyubarsky 99, Nakamura & Meier 04**)
- Dominant modes of the Z-pinched instabilities are kink (m=1) and pinch (m=0) ones. They may be stabilized by the large-scale longitudinal MF component (if strong enough).

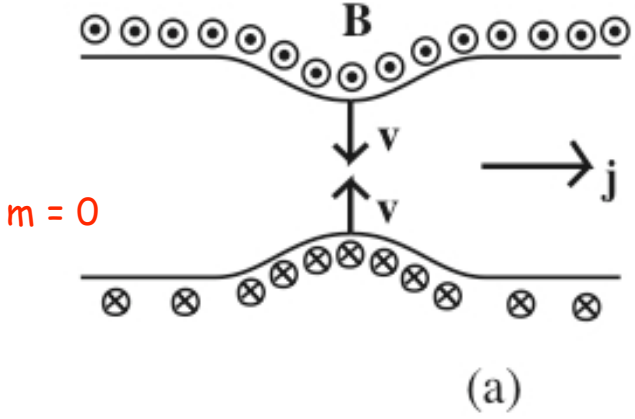

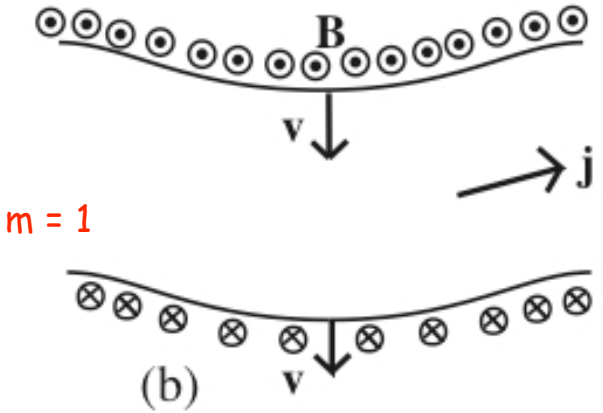

Blazar Phenomenon

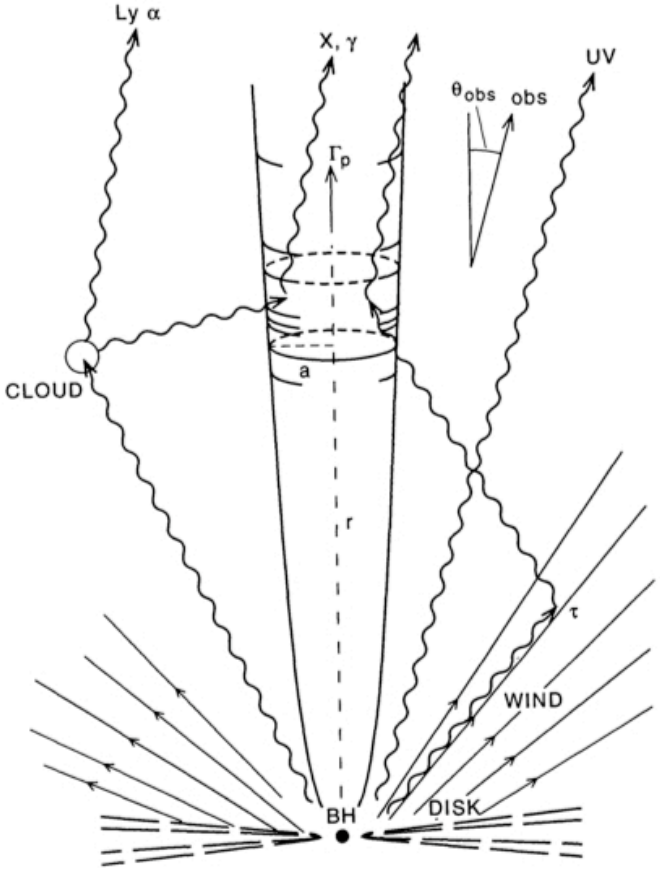

Modeling of the broad-band blazar emission (and its variability) in a framework of the leptonic scenario (**Dermer & Schlickeiser 1993, Sikora, Begelman & Rees 94, Blandford & Levinson 95)** allows to put some constraints on the physical parameters of the blazar emission region. In particular, such modeling indicate that:

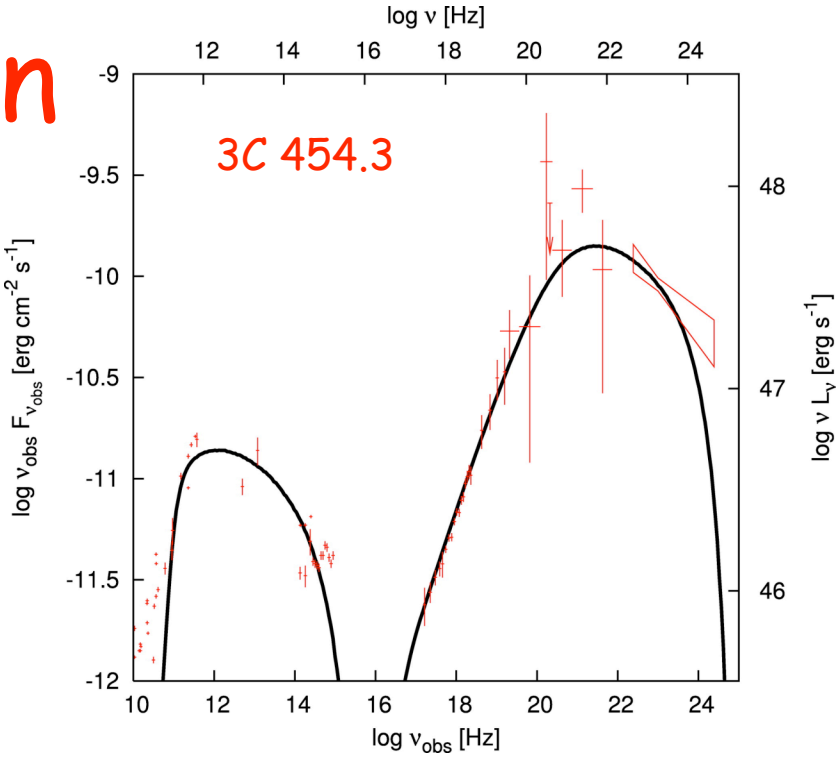

1) Emission regions are compact, R ~ 10^{16} cm .
2) Implied highly relativistic bulk velocities of the emitting regions, Γ ~ 10-30 , are in agreement with the ones inferred from the observed superluminal motions of VLBI jets on pc (kpc?) scales.
3) Energy density of MF is typicaly slightly below energy density of radiating ultrarelativistic electrons, $U_B \leq U_{e,rel}$.
4) The implied MF intensity B ~ 0.1-1 G is consistent with the one inferred from the SSA features in flat spectra of compact radio cores.

Jet Power

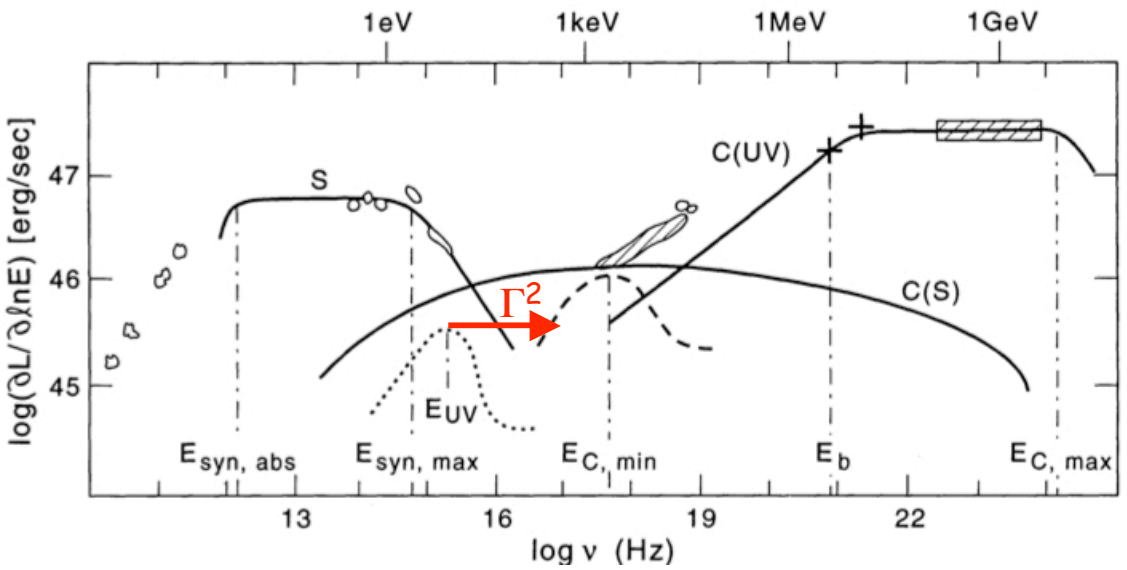

In addition, the power carried by ultrarelativistic electrons cannot account for the total radiated power of blazars, or for the kinetic power of quasar jets deposited far away from the active nucleus (e.g., **Celotti & Ghisellini 08**). So either

(1) MF is dominating dynamically, while blazar emission is produced in small jet sub-volumes with MF intensity lower than average (?), or

(2) jets on blazar scales are dynamically dominated by protons and/or cold electrons.

However, lack of bulk-Compton features in soft-X-ray spectra of blazars (**Begelman & Sikora 87**, **Sikora+97**, **Sikora & Madejski 00**, **Moderski+04**, **Celotti+07**) indicates that

(3) cold electrons cannot carry bulk of the jet power (at least in the luminous, quasar-type blazars)

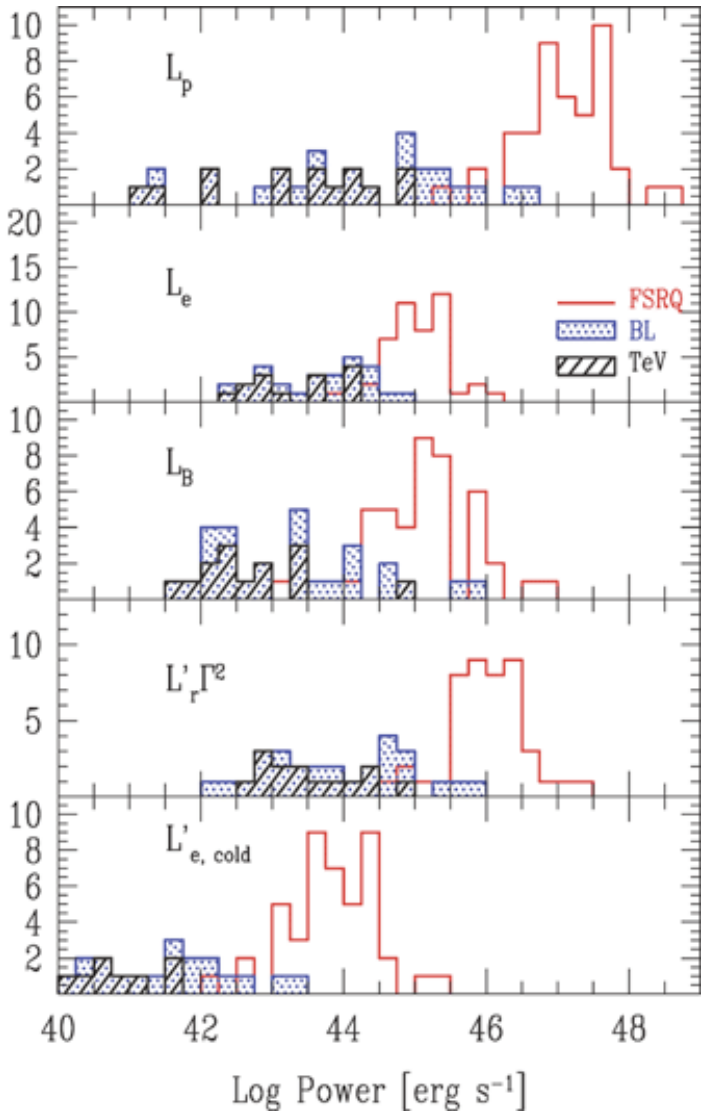

Powerful Blazars: Shock Spectra

In the "internal shock model" (**Sikora+94, Spada+01**) one should expect blazar emission zone located at the distances
$r \sim \Gamma^2 r_g \sim (10^2 - 10^3) r_g \sim 0.01\text{-}0.1$ pc .

In the "reconfinement shock model" (**Sikora+07, Sikora+09**) one can expect the blazar emission zone located at larger distances
$r \sim 1$ pc .

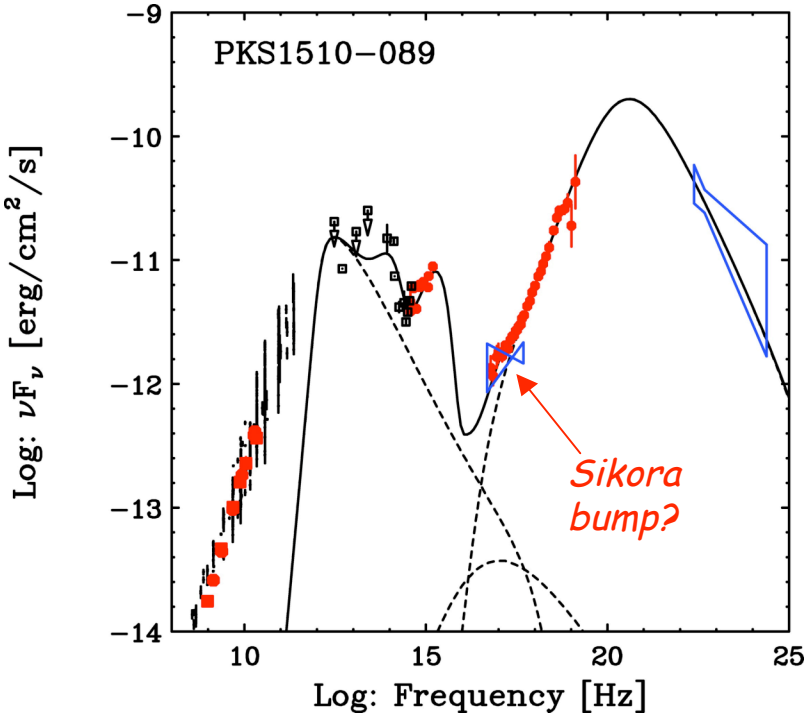

The implied physical pramaters of the blazar emission zone, as well as the spectral energy distribution of the emitting ultrarelativistic electrons (being consistent with the shock acceleration scenario - **though not the `standard' diffusive shock acceleration model!**) suggest that the extragalactic jets are matter (proton) dominated already at sub-pc scales.

Kataoka+08: parameters of blazar PKS 1510-089
$\Gamma \sim 20$, $r \sim 1$ pc , $R \sim 10^{16}$ cm ,
$N_e/N_p \sim 10$, $B \sim 0.6$ G
$L_p \sim 2 \times 10^{46}$ erg/s , $L_e \sim 0.1 \times 10^{46}$ erg/s , $L_B \sim 0.6 \times 10^{46}$ erg/s

$N_e(\gamma) \propto \gamma^{-1.35}$ **for** $\gamma < \gamma_{br} \sim 100$
$\propto \gamma^{-3.35}$ **for** $\gamma > \gamma_{br} \sim 100$

Helical VLBI Jets?

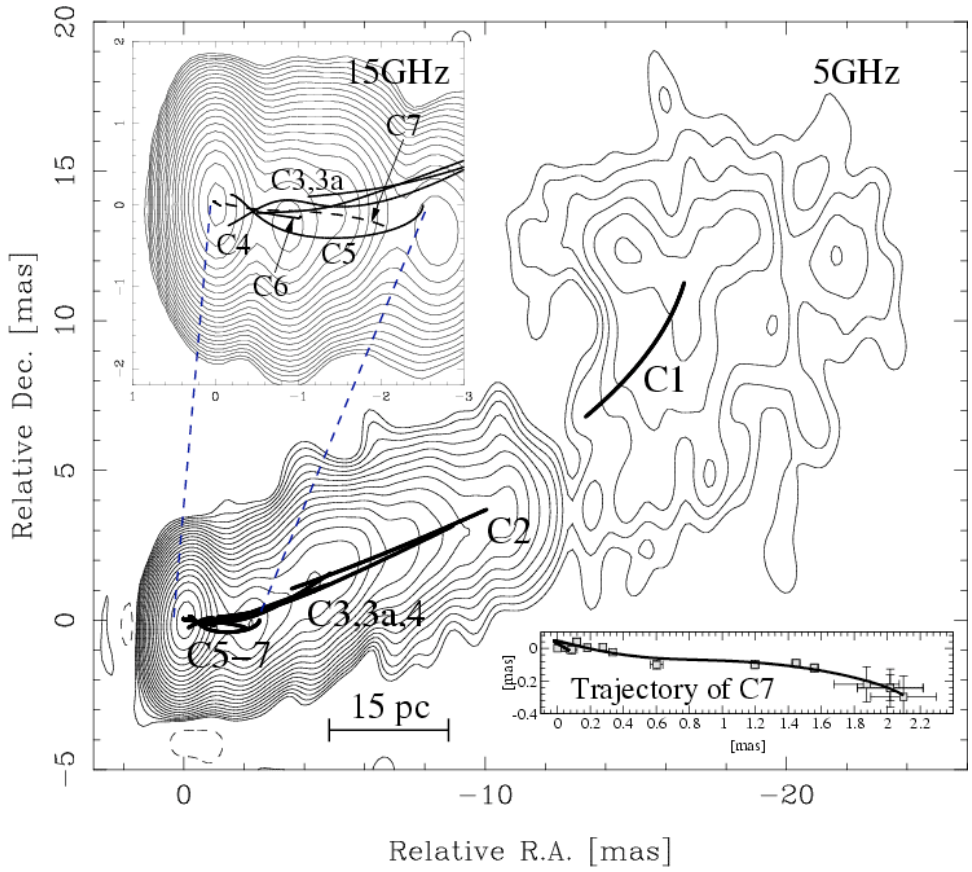

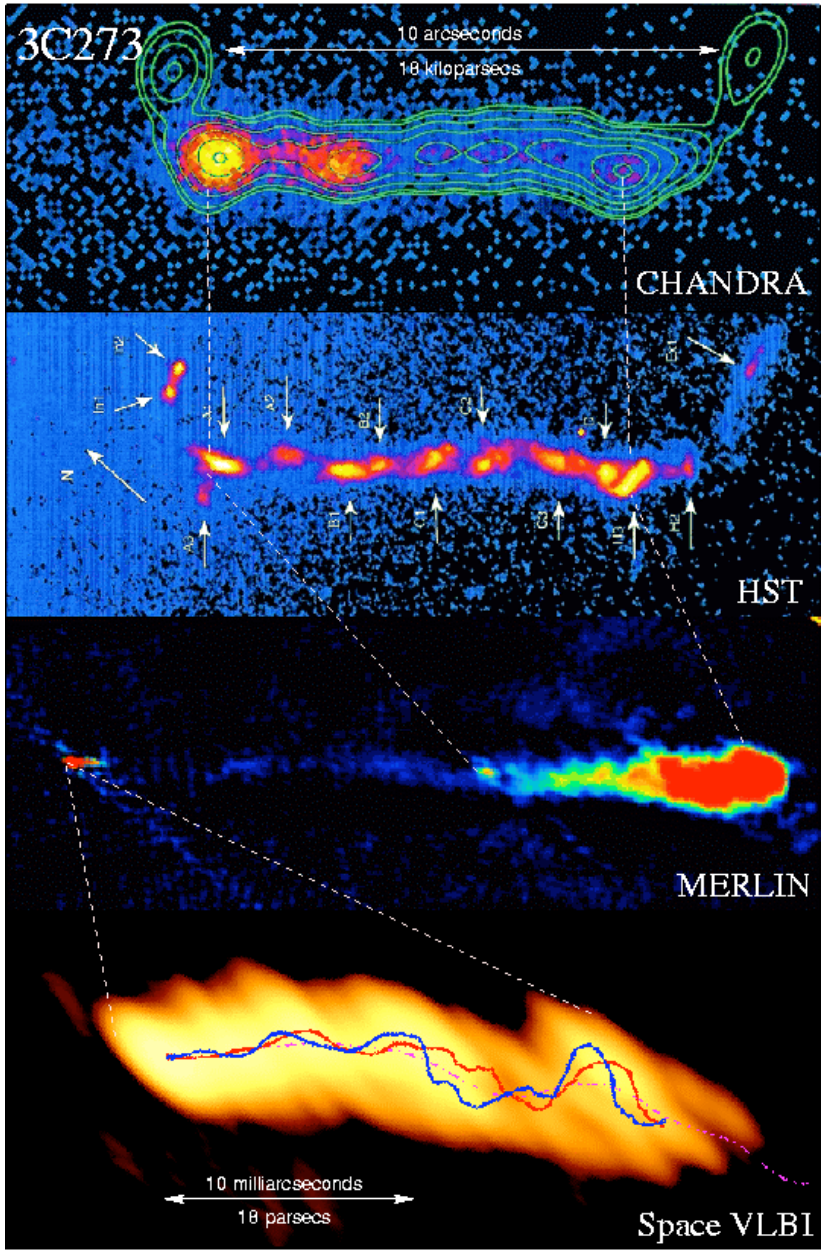

Lobanov & Zensus 01, Lobanov & Roland 05: "helical" trajectories of VLBI blobs on pc-scales in 3C 345 and 3C 273. If true, may be due to the dominant helical MF, but may also reflect Kelvin-Helmhotz instabilities in matter-dominated jets (**Hardee 07, Perucho+07**).

Slowly Accelerating VLBI Jets?

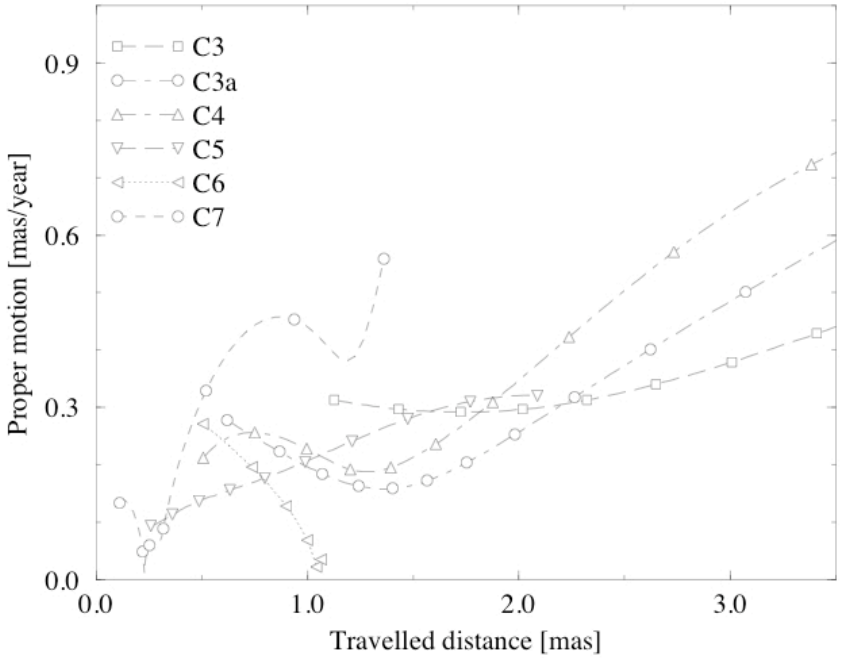

Unwin+97, Lobanov & Zensus 99, Cotton+99, Homan+01, Piner+03: in some cases gradual acceleration of VLBI blobs on >pc scales is observed. However, is it the same blob observed, or different blobs at different distances from the center? Other objects show variety of blobs' apparent velocities, from super- to sub-luminal, including stationary features (**Jorstad+01, Cohen+07**).

Lobanov & Roland 05: 3C 345

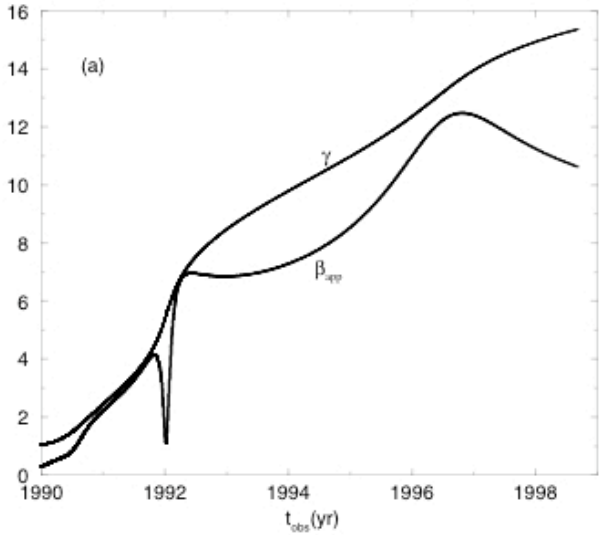

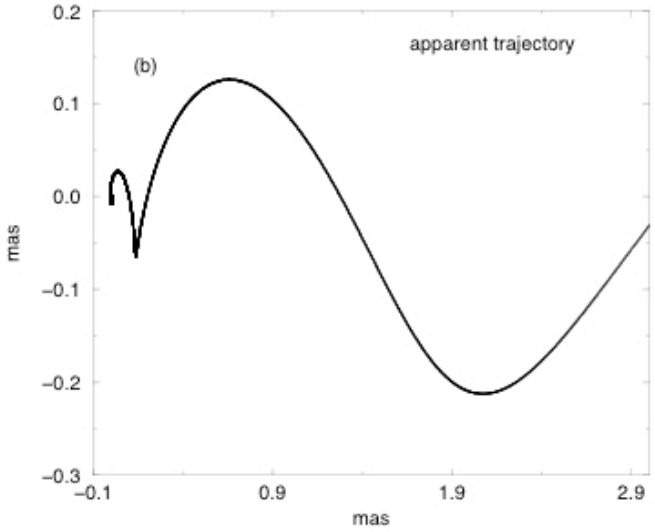

Should we expect magnetic acceleration at work at such large distances from the core, corresponding to $>10^5\ r_g$?

Slowly Collimating VLBI Jets?

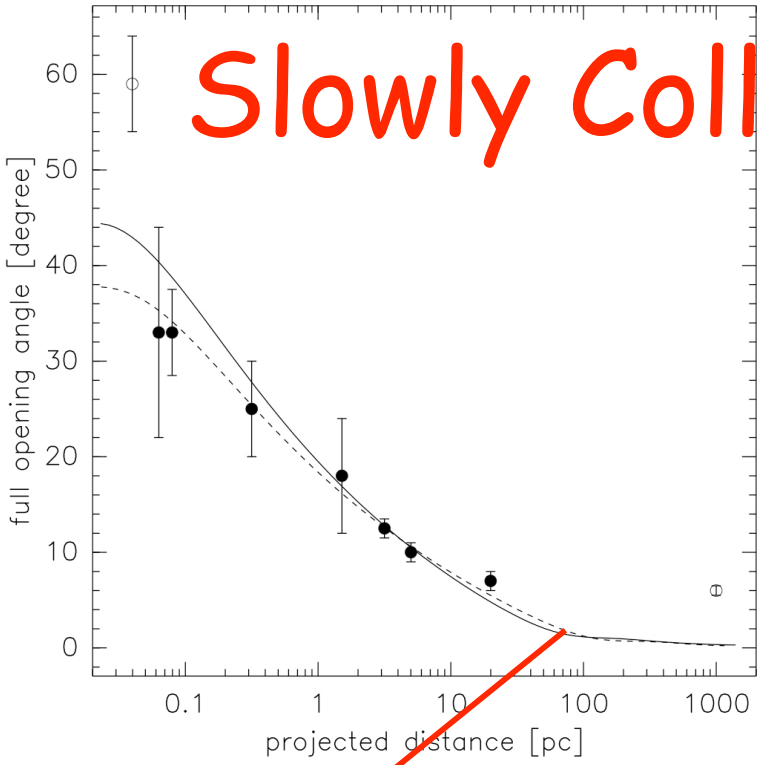

Gracia+05,08, Zakamska+08: MHD models provide very good fits to the observed gradual change of the jet opening angle along M87 jet up to 100 pc distances from the center. In addition, radio flux profiles (both along and across the jet) may be also explained.

However, hydrodynamical models involving reconfinement of a matter-dominated jet by the ambient medium work as well (**Stawarz+06, Cheung+07**).

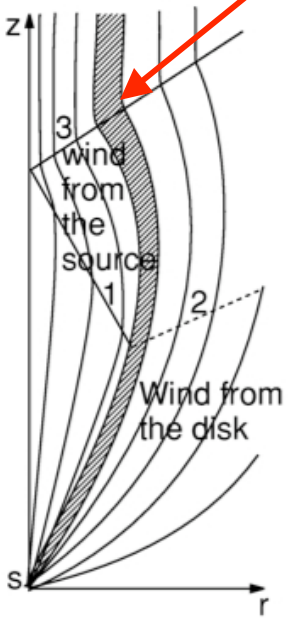

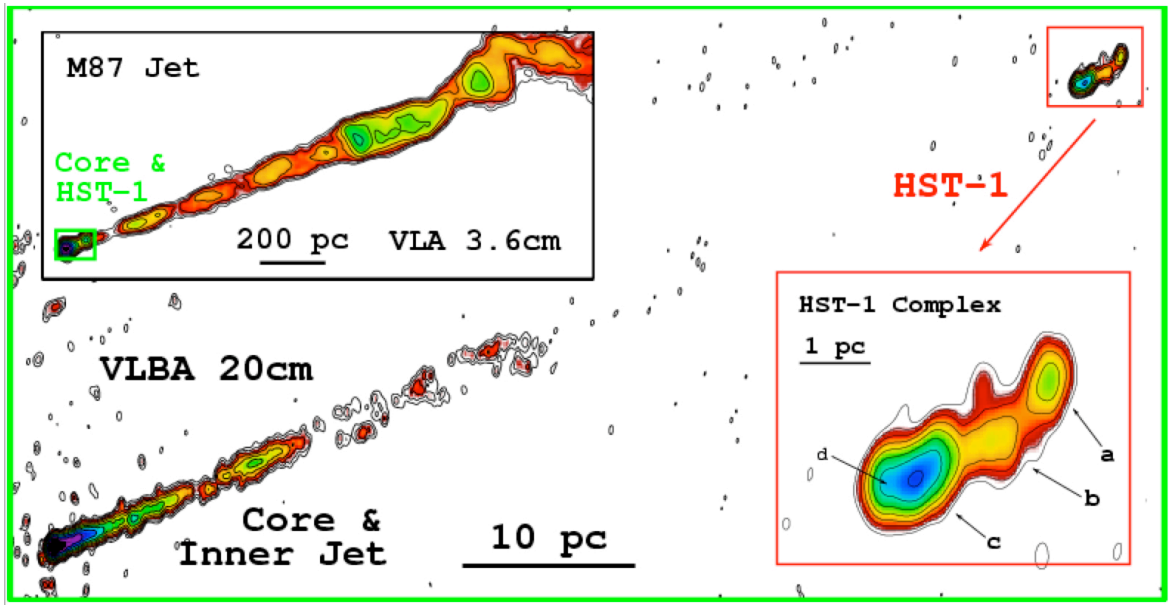

H.E.S.S. Observations of M87

First detected by HEGRA.
Later observed by H.E.S.S. (**Aharonian+07, for the HESS Collab.**). Recently detected also By MAGIC and VERITAS.

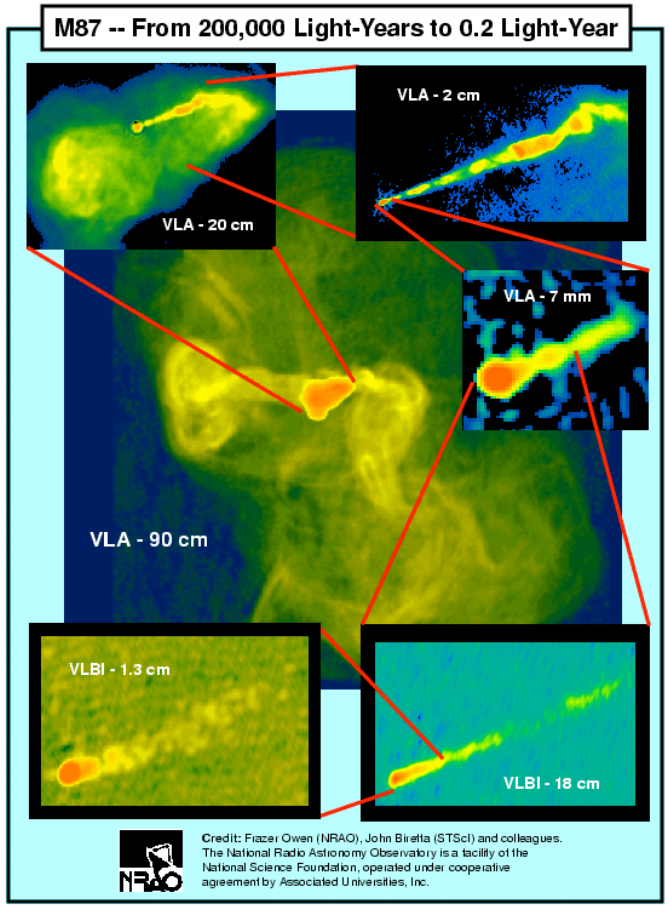

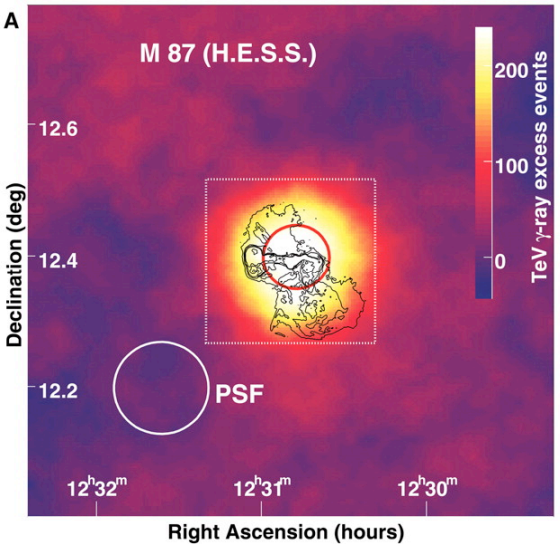

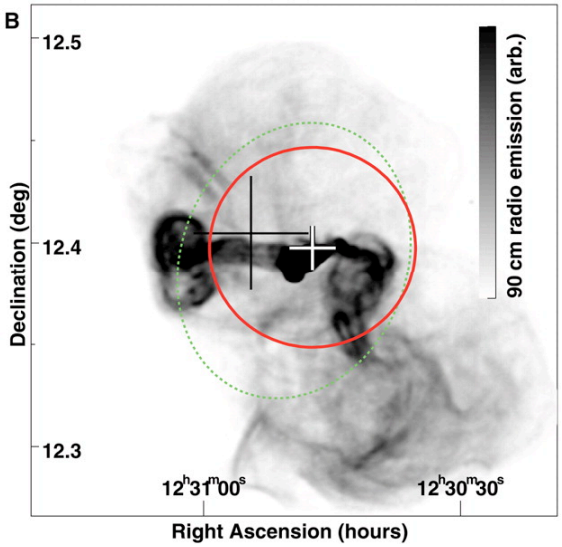

What can be the source of the TeV emission detected from M87?

- Inner (sub-pc scale) jet?
- Large-scale (kpc-scale) jet?
- Virgo A cluster?
- Central SMBH ($M_{BH} \sim 3\times10^9\ M_{sun}$) ?

Only the ~kpc-scale jet is the guarantee TeV emitter, because it is known to accelerate electrons up to TeV energies (synchrotron X-rays with B~0.1-1 mG!).

Variable TeV Emission from M87

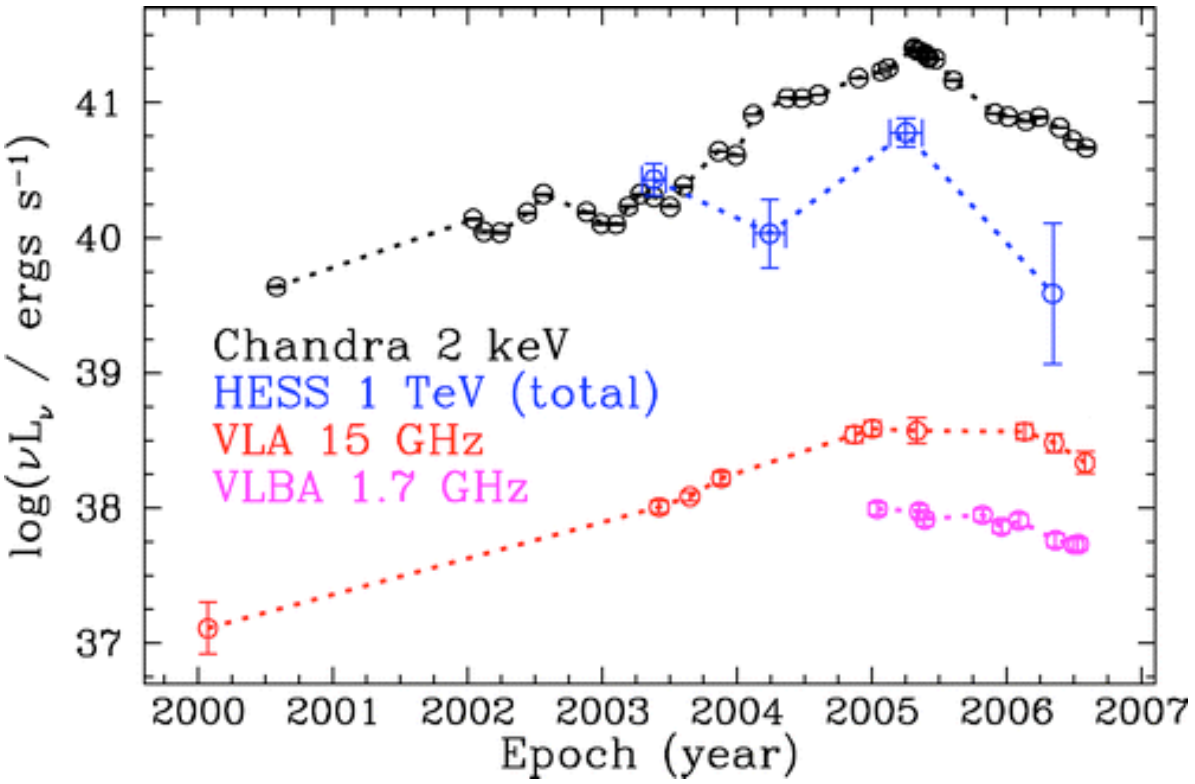

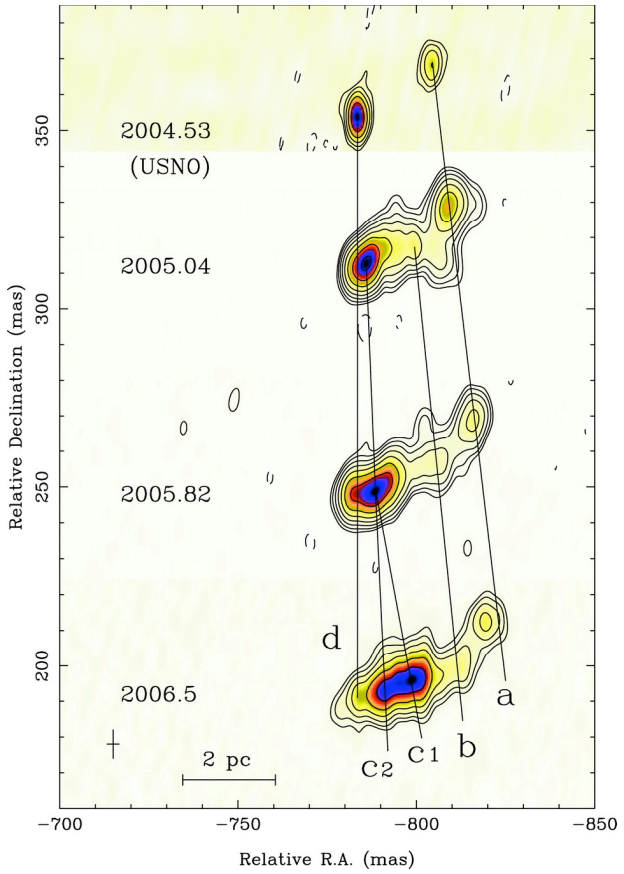

Short variability of the TeV emission observed from M87 implies linear size of the emission region $R_\gamma < 0.002\ \delta$ pc $\sim 10\ \delta\ R_g$ **(Cheung, Harris & Stawarz 07)**.

HST-1 knot:
$r \sim 100$ pc $\sim 10^6\ R_g$
$R_{HST} < 0.15$ pc
$R_X < 0.02\ \delta$ pc
$\delta > 2$

Polarization of pc-Scale Jets

- Radio-to-optical polarization of blazars indicate typically B⊥ for the unresolved cores (especially in the case of BL Lacs), and variety of configurations for the resolved sub-pc scale jets (**Impey+91, Cawhorne+93, Gabuzda & Sotho 94, Cawthorne & Gabuzda 96, Stevens+96, Nartallo+98, Gabuzda+00, Lister & Homan 05, Jorstad+07**).
- B⊥ may indicate compression of the tangled magnetic field by shocks, while B|| shearing of the tangled magnetic field due to velocity gradients (**Laing 80, 81, Hugh+89**). This would be consistent with matter-dominated outflows.
- B⊥ could also be due to the dominant toroidal MF. Such interpretation is consistent with B⊥ observed at the spatially extended regions where the jets bend, and also with the observed altering B⊥- B|| structures (**Gabuzda+04**).
- Interpretation of the blazar polarization data is complicated and in some cases not conclusive due to the relativistic effects involved (**Lyutikov+05**).

Spine-Shear Layer Structure

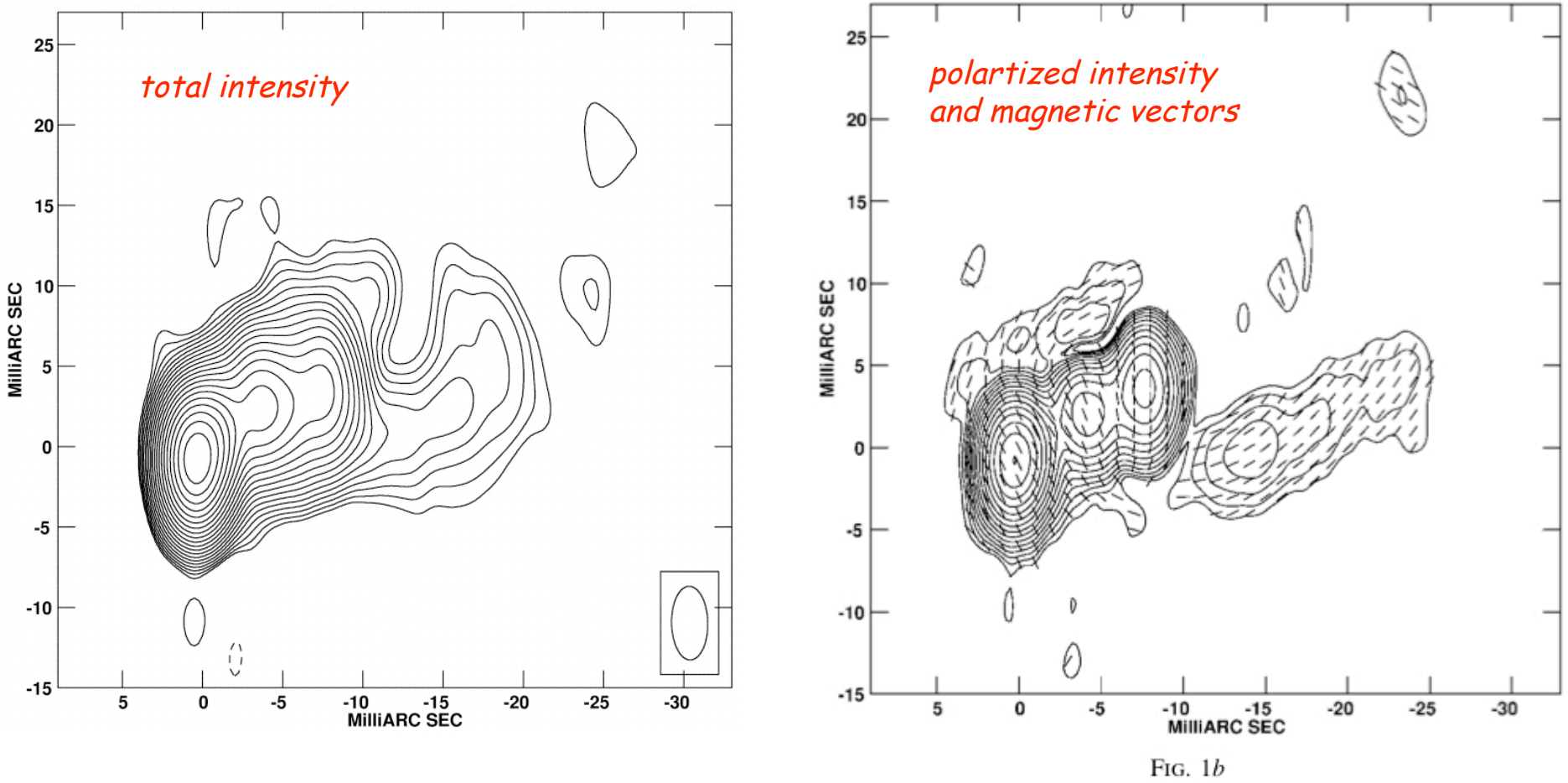

FIG. 1*b*

Attridge+99: Spine B⊥ / boundary layer B|| structure in 1055+018.
Shock compression/velocity shear in the matter-dominated jet,
or helical MF in the current-carrying outflow?
(Similar cases: **Gabuzda+01**, **Pushkarev+05**)

RM Gradients: Expected

$$c^2 k^2 = \zeta \omega^2$$

$$\zeta = 1 - \frac{\omega_{\rm pl}^2}{\omega\,(\omega \pm \omega_{\rm L})}$$

$$v_{\rm ph} = \frac{\omega}{k} \quad , \quad v_{\rm gr} = \frac{\partial \omega}{\partial k}$$

$$\Delta\chi = \frac{2\pi\, e^3}{m_{\rm e}^2 c^2\, \omega^2} \int_0^L n_{\rm th}\, B_{0,\parallel}\, ds$$

$$\left(\frac{\Delta\chi}{\rm rad}\right) = RM \cdot \left(\frac{\lambda}{\rm m}\right)^2$$

$$RM = 0.81 \int_0^L \left(\frac{n_{\rm th}}{\rm cm^{-3}}\right) \left(\frac{B_{0,\parallel}}{\mu\rm G}\right) \left(\frac{ds}{\rm pc}\right)$$

When propagating through a magnetized plasma ("external screen"), a polarized wave experiences rotation of a plane of polarization. That is because any plane polarized wave can be treated as a linear superposition of a right-hand and left-hand circularly polarized component. Circularly polarized wave with positive helicity has different phase velocity than the wave with negative helicity within the magnetized environment.

RM gradients across a jet should be expected in the case of a helical magnetic field (**Blandford 93**)

Gabuzda 06

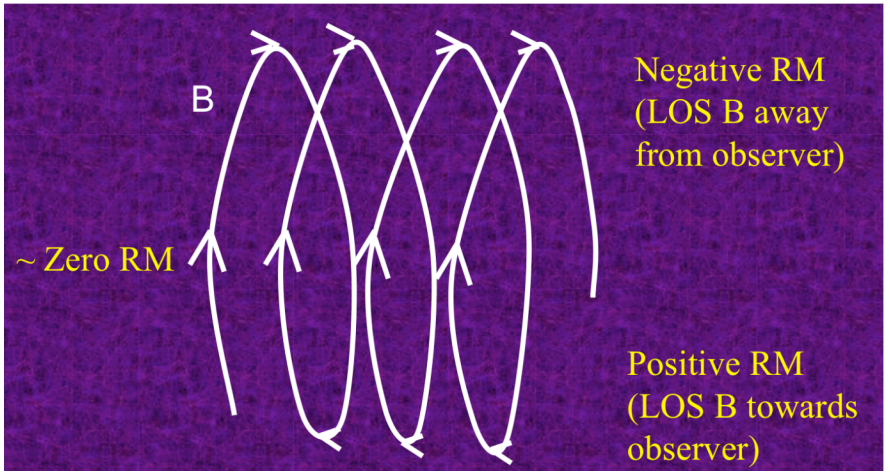

RM Gradients: Observed, Variable

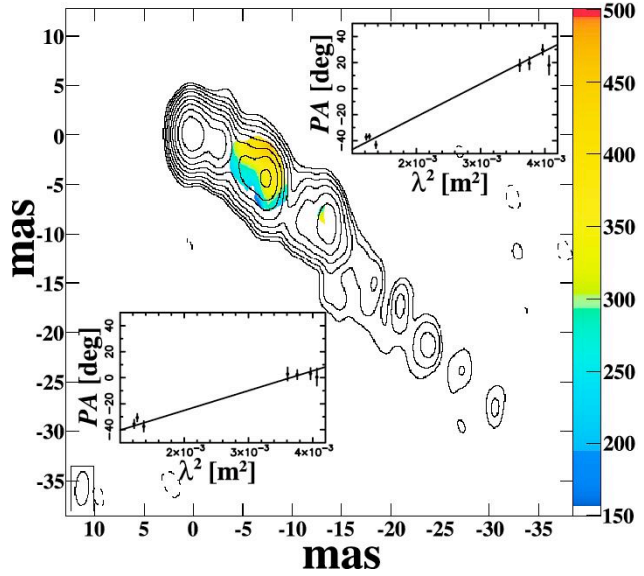

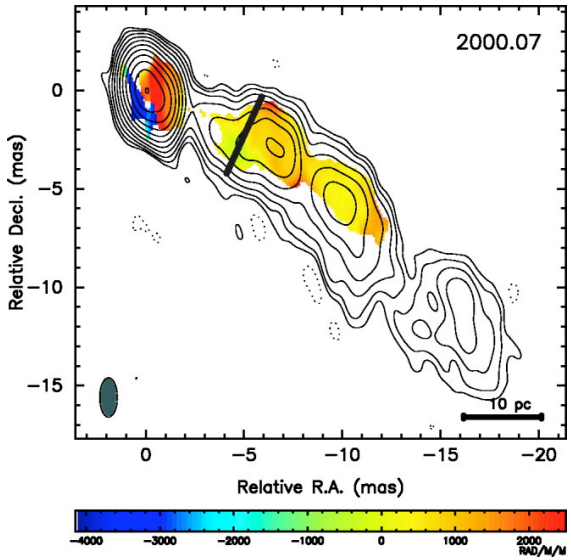

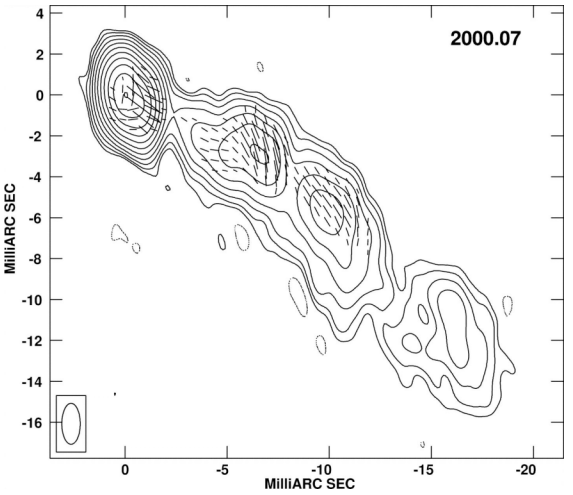

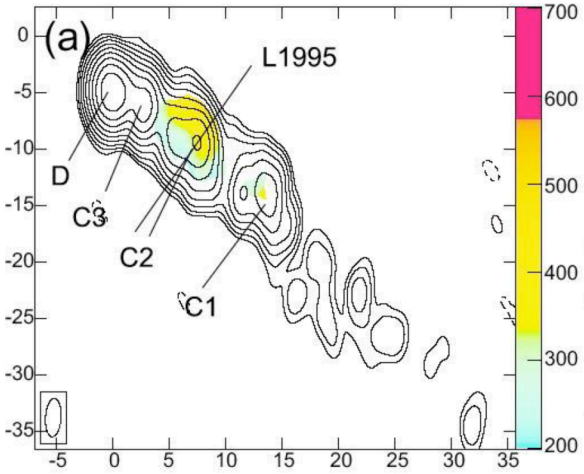

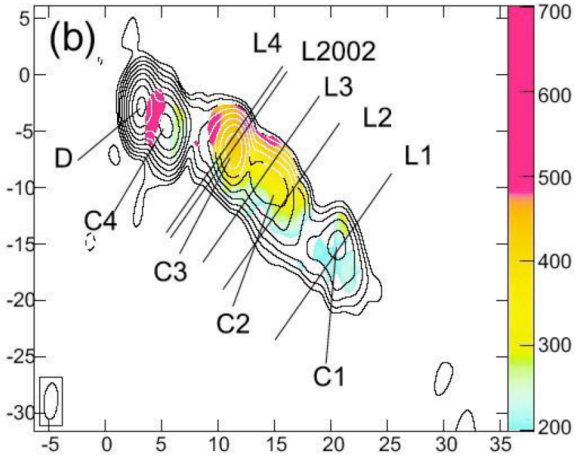

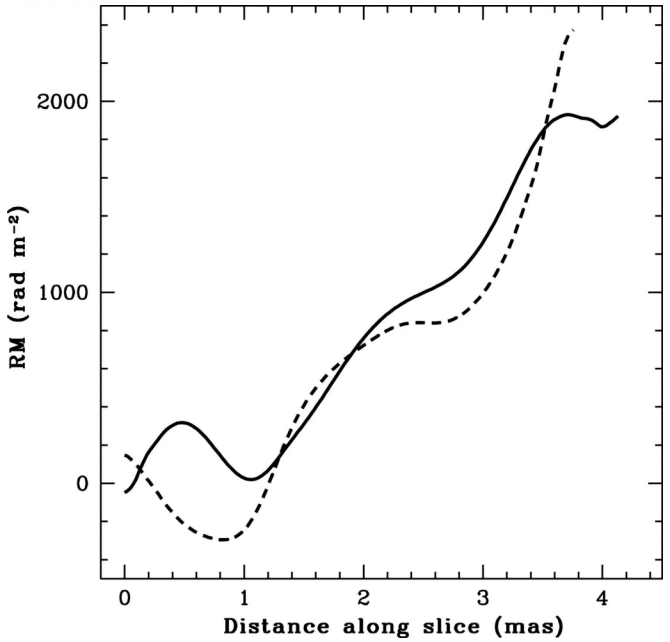

3C 273: **Asada+02, 08, Zavala & Taylor 05**

(other examples: **Gabuzda+04**)

Where Is Faraday Screen?

Faraday screen has to be external to the emitting region because:

- Rotations >45deg sometimes observed (**Sikora+05**).
- RM gradients sometimes localized where the jet interacts with the clouds of ISM (3C 120; **Gomez+00, 08**).
- λ^2 dependence always holds.
- Decrease of RM along the jets observed (**Zavala & Taylor 02, 03, 04**).
- High fractional polarization observed from the RM gradient regions.

Faraday screen cannot be completely unrelated to jet because:

- RM gradients vary on timescale of years (**Zavala & Taylor 05, Asada+05**).
- Direction of RM gradients always agrees with a sign of a circular polarization observed (**Gabuzda+08**)*.

Spine/Sheath structure again?

**CP may result from Faraday conversion of LP mediated by helical MF. The sign of CP is then determined by the helicity of MF, and so should agree with the direction of the RM gradient.*

Kpc-Mpc Scales

- In the case of a matter-dominated jet, when the MF is frozen-in to the fluid, one expects $B_T \propto r^{-1}$ and $B_P \propto r^{-2}$ (conservation of MF energy flux and MF flux; **Begelman+84**). Thus, the toroidal MF should dominate over the poloidal one on large scales. This simple scalling is roughly consistent with the equipartition MF intensity:

$B_{eq} \sim B \sim B_{blaz}\,(pc/100kpc) \sim B_E\,(r_g/100kpc) \sim 1\text{-}10\mu G$

- However, polarimetry of large-scale jets in powerful quasars and radio galaxies indicate B||. This may suggest action of a velocity shear (re)-orienting MF lines (**Laing 80, 81**). The regions with strong velocity shear are likely to be the sites of the enhanced magnetic reconnection, dynamo action, and injection of turbulence, and therefore of the enhanced particle acceleration/energy dissipation (**De Young 86**).
- Note that the longitudinal MF component cannot be unidirectional on large scales, since this would imply too large magnetic flux: $B_{eq}\,(kpc)^2 \gg B_E\,r_g^{\,2}$. Thus, B|| must indeed reverse many times across the jet (**Begelman+84**).

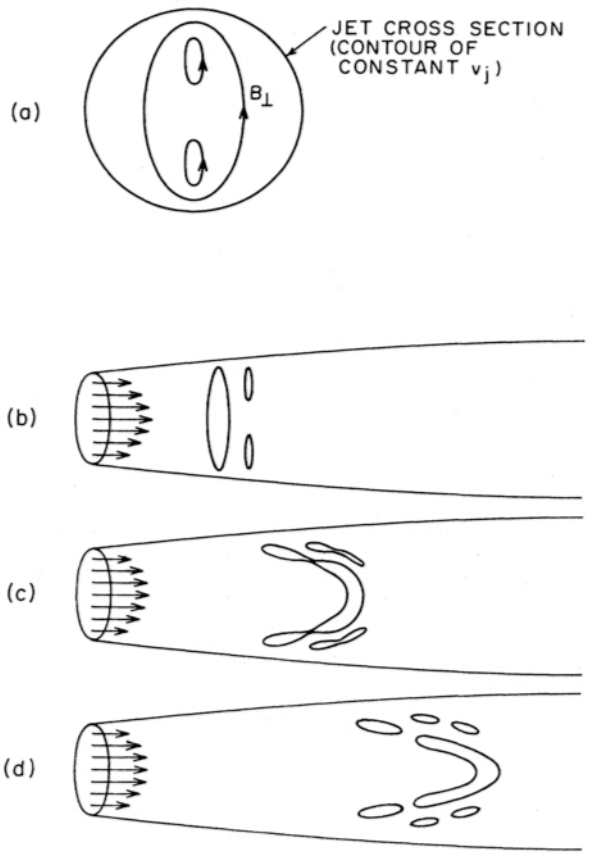

Begelman+84

FR I Jets

2-kpc-long jet in M87 radio galaxy (d_L = 16 Mpc) observed at radio, optical, and X-ray frequencies.

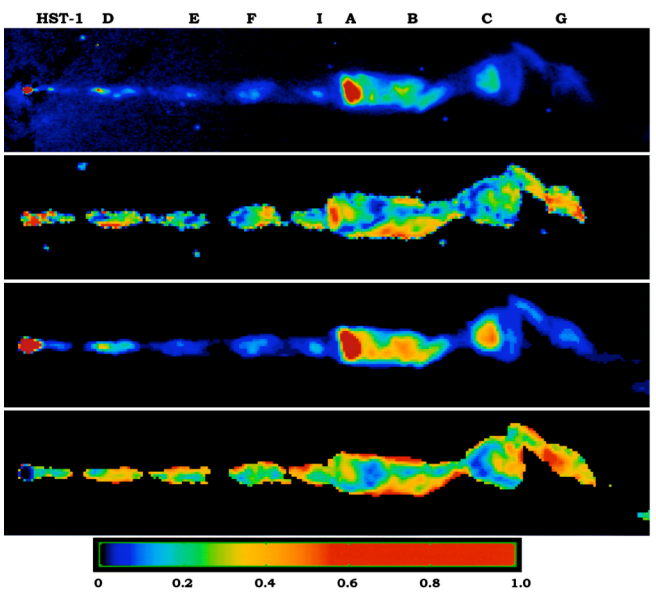

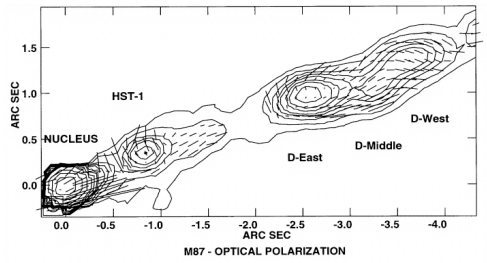

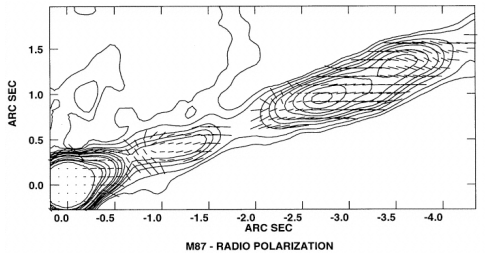

Perlman+99

Radio and optical polarized emission: internal structure consistent with the spine – boundary shear layer morphology, and so matter-dominated outflow.

Radio-to-X-ray synchrotron emission:

- presence of $\gamma = 10^8$
- electrons (E_e = 100 TeV);
- broad-band knots' spectra hardly consistent with the standard shock acceleration models;
- a need for continuous electron acceleration along the whole jet ($\ell_{rad,\,X} \sim 10$ pc « 2 kpc).

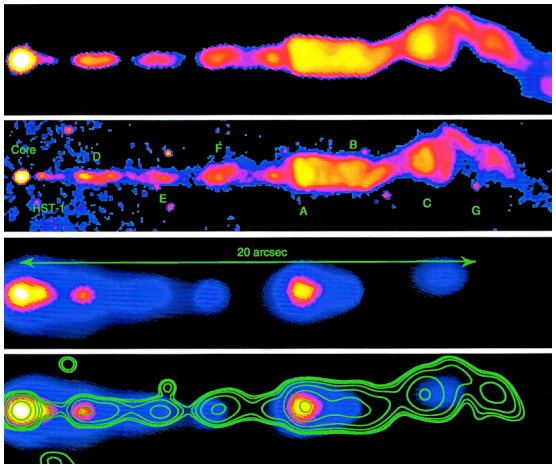

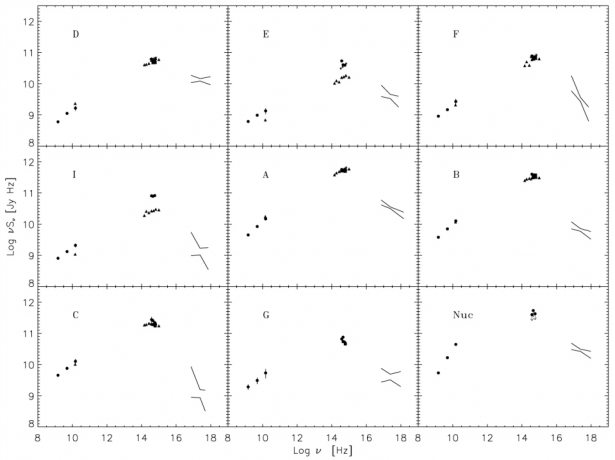

Marshall+02, Wilson & Young 02

Jet Confinement

- Jets with toroidal MF can be self-confined due to magnetic tension involved: $B_T^2/4\pi = p_j$ (**Benford78, Chan & Henriksen 80, Bicknell & Henriksen 80, Bridle+81**).
- Toroidal MF implies a net current flowing along the jet, $B_T \sim 2I/cR_j$. If the ambient medium behaves as a perfect conductor, the return current is induced on the interface between the cocoon and the ambient medium (or throughout the cocoon, and/or on the surface of the jet), such that $p_{ext} \sim p_j (R_j/R_{ret})^2$ (highly overpressured jets, underpressured cocoons!).
- If shear effects are important, the force-free equilibrium may establish: magnetic tension (B_T) confines highly overpressured (B_P) jet spine.

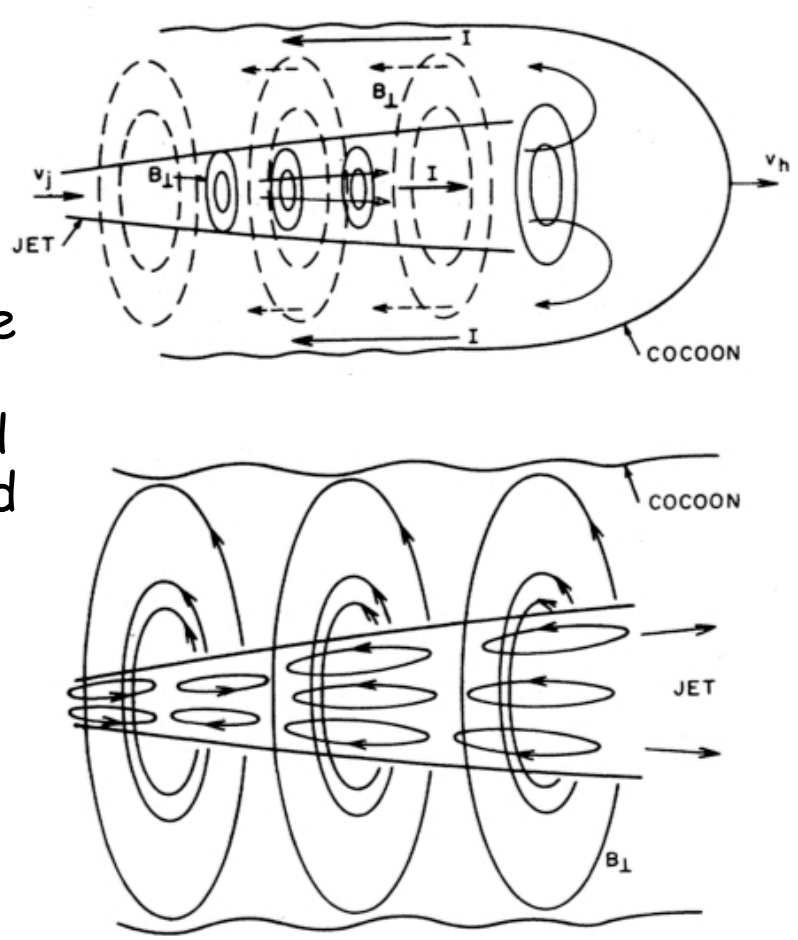

Begelman+84

Large-Scale Morphology

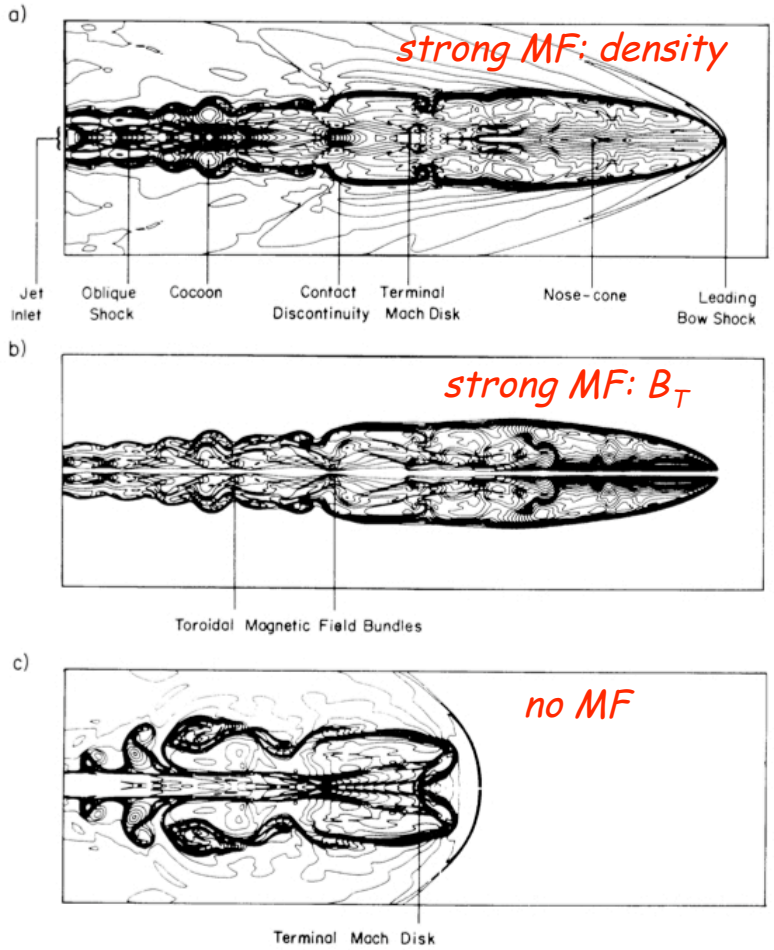

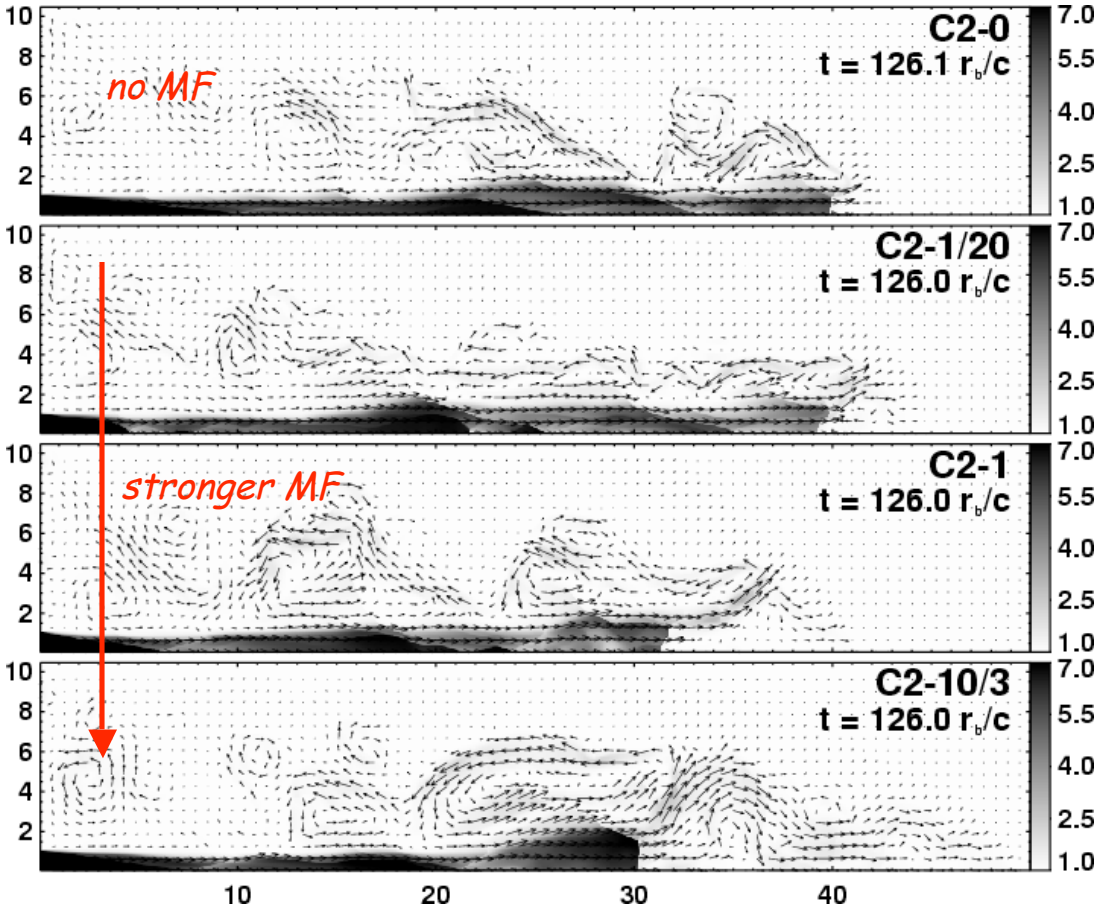

Clarke+86, Lind+89, Kossl+90, Komissarov 99, Leismann+05: 2D axisymmetric ideal MHD simulations of strongly magnetized jets (with no substantial poloidal MF) reveal thin ("no-backflow") cocoons and "nose-cone" morphology of jet termination regions (different from hydro jets!).

Nose-Cone Structures

Contact discontinuity: here the return current flows (in the case of an ideal MHD).

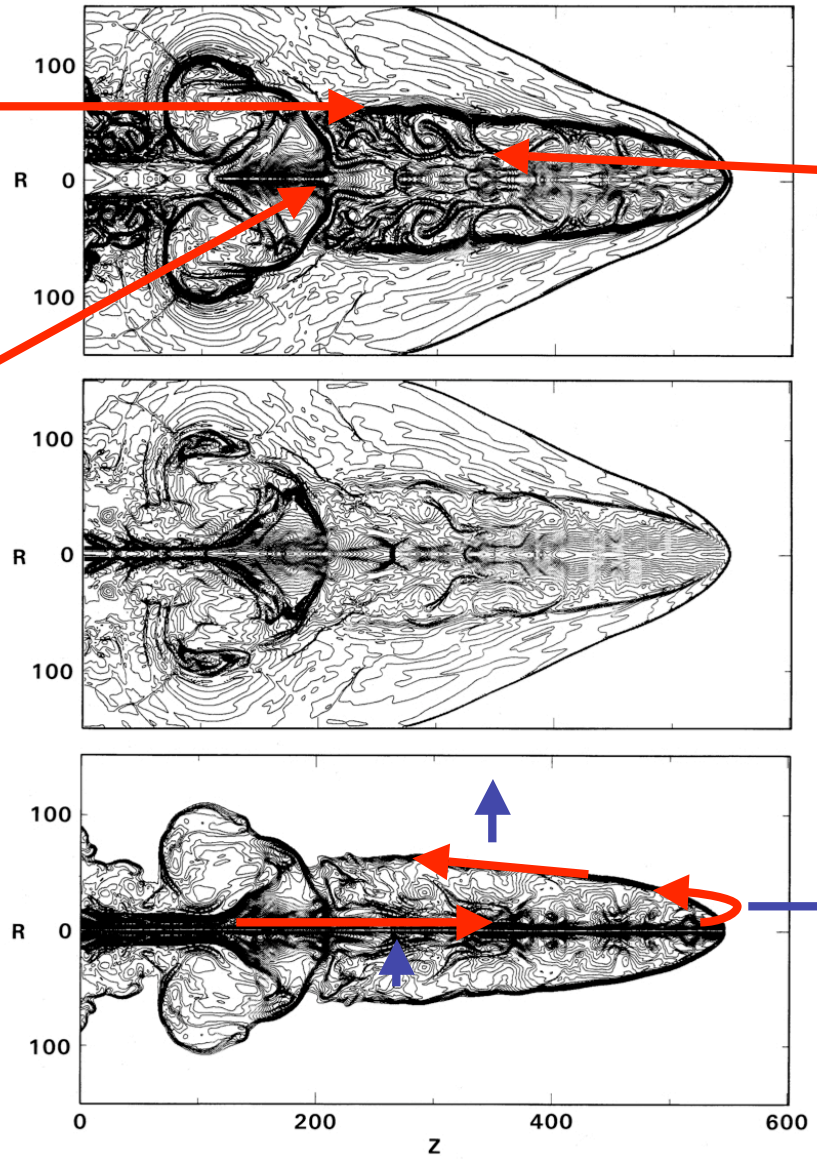

"Nose": here the current-carrying plasma is confined by the self-induced toroidal MF which also prevents any backflow.

Mach disk: here most of the fluid kinetic power is thermailzed.

The Lorentz force $\mathbf{j} \times \mathbf{B}_T$ pinches (collimates) the jet, drives expansion of the jet head, and drives expansion of the cocoon.

Is it consistent with observations?
Is it not an artifact of the 2D axisymmetric simulations? (no reconnection!)

Lind+89: matter density, gas pressure, magnetic field

FR II Radio Galaxies

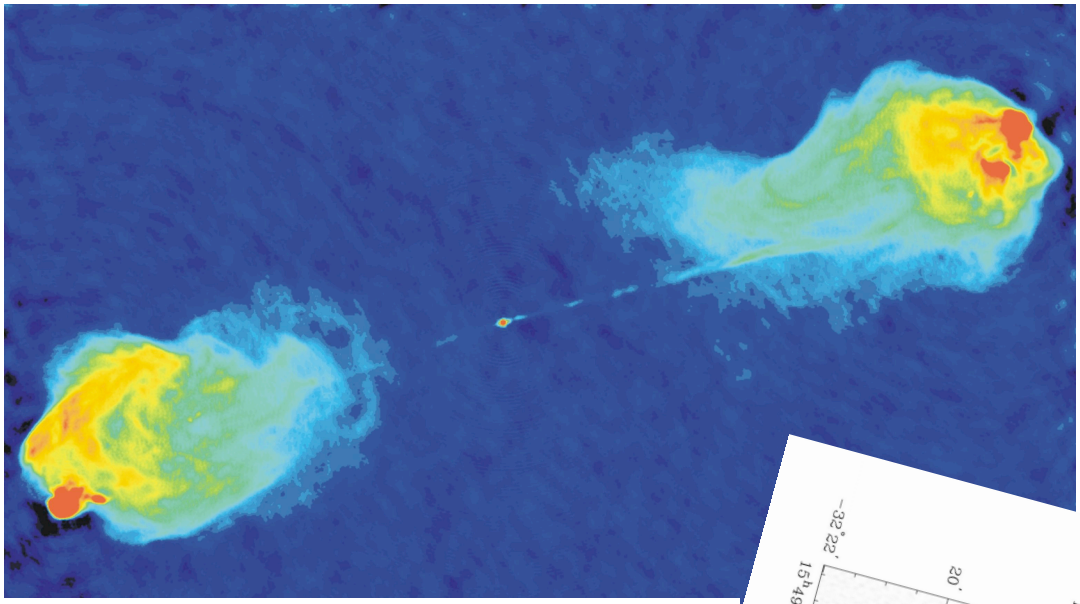

Classical FR II morphology (e.g., Cygnus A; **Carilli & Barthel 96**) is consistent with matter-dominated jet (fat lobes, no nose-cones, substantial backflows).

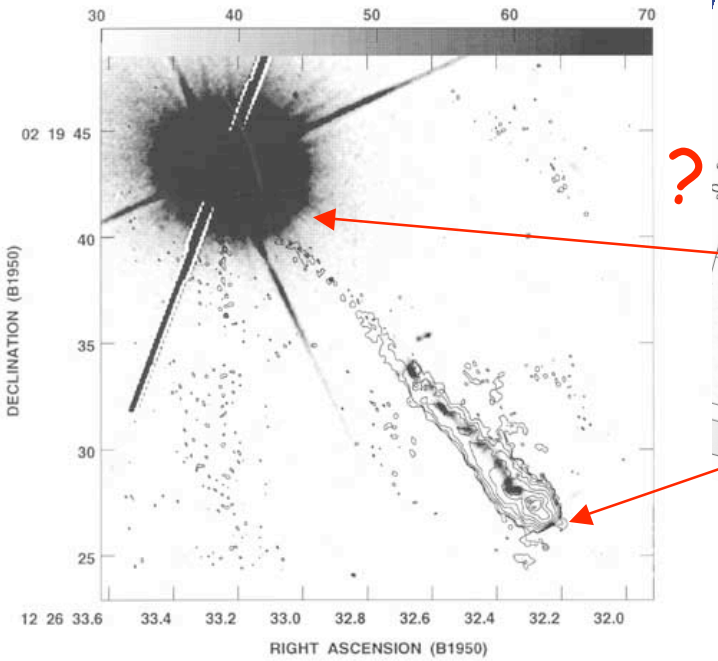

?

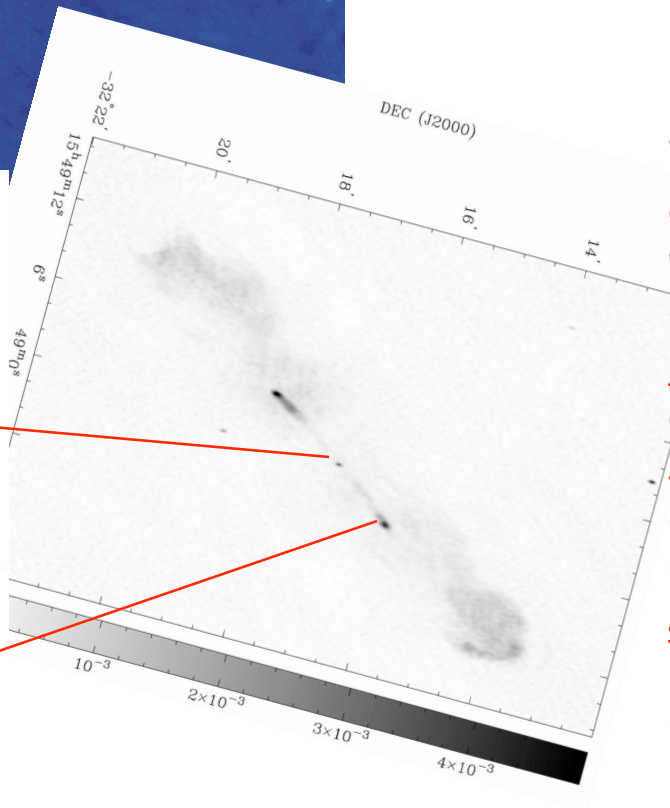

"Problematic" cases of one-sided jets/lobes with narrow cocoons (e.g., 3C 273, **Bahcall+95**) can be explained as inner structures of double-double radio sources (e.g., PKS B 1545; **Saripalli+03**), without invoking strong MF (**Stawarz 04**).

Chandra Quasar Jets

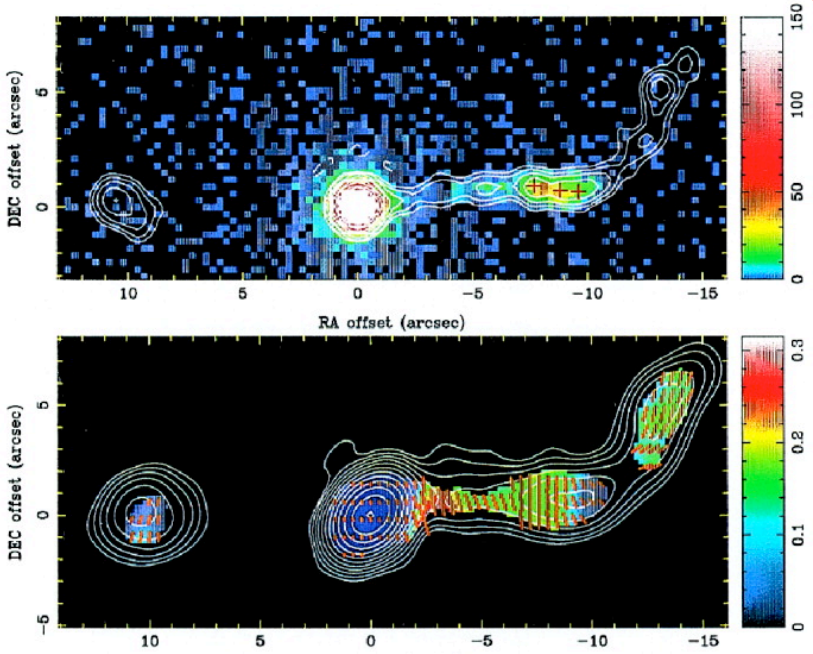

Chandra X-ray Observatory detected surprisingly intense X-ray emission from large-scale (100 kpc – 1 Mpc) quasar jets (L_X ~ 10^{44}-10^{45} erg/s). Many examples (e.g., **Schwartz+00**, **Cheung+**, **Hardcatle+**, **Harris+**, **Jorstad+**, **Kataoka+**, **Kraft+**, **Marshall+**, **Sambruna+**, **Siemiginowska+**).

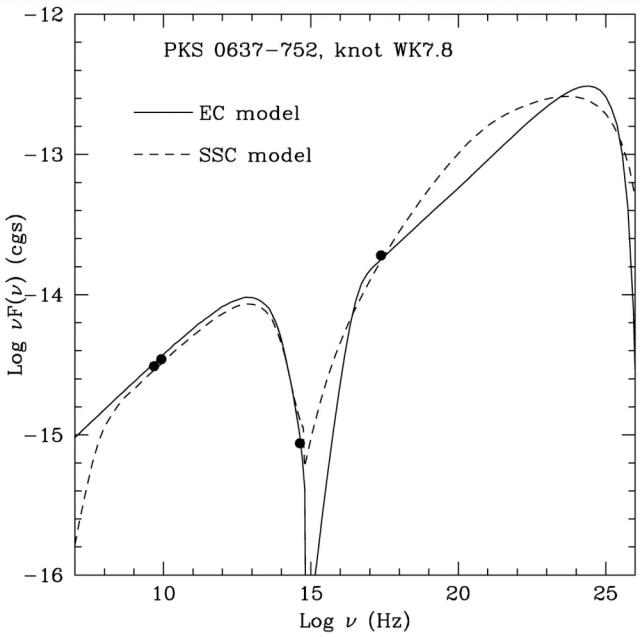

It was proposed that this X-ray emission is due to inverse-Compton scattering of the CMB photons by low-energy jet electrons, E_e ~ 100 MeV. (**Tavecchio+00**, **Celotti+01**).

IC/CMB model requires highly relativistic bulk velocities ($\Gamma > 10$) on Mpc scales, and dynamically dominating protons,

$L_p > L_e \sim L_B$

with $B \sim B_{eq}$ ~ 1-10 μG. Note that for $\Gamma<10$ the IC/CMB model would imply $B << B_{eq}$

Non-standard Electron Spectra?

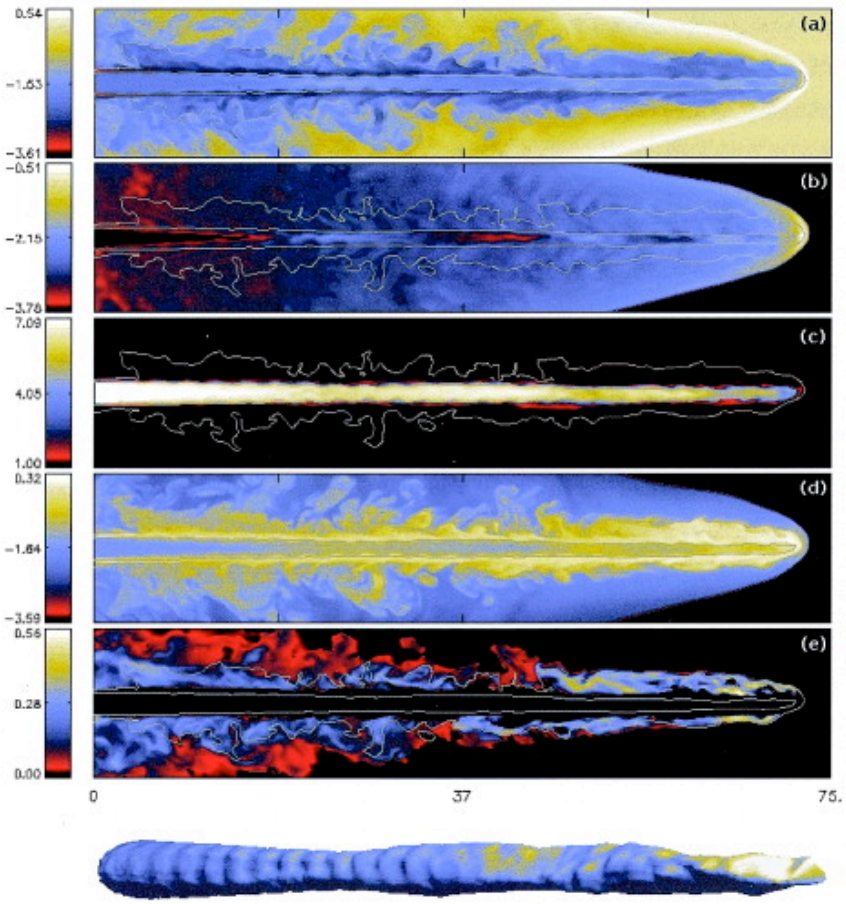

Relativistic 3D-HD simulations indicate presence of highly turbulent shear boundary layers surrounding relativistic jets **(Aloy+99)**.

Relativistic large-scale jets are highly turbulent, and velocities of turbulent modes thereby may be high. As a result, stochastic (2nd order Fermi) acceleration processes may be dominant. Assuming efficient Bohm diffusion (i.e. turbulence spectrum $\delta B^2(k) \propto k^{-1}$), one has

$$t_{acc} \sim (r_g/c)\,(c/v_A)^2 \sim 5 \times 10^2\ \gamma\,[s]$$
$$t_{esc} \sim R_j^2/\kappa \sim 6 \times 10^{24}\ \gamma^{-1}\,[s]$$
$$t_{rad} \sim 6\pi m_e c\ /\ \sigma_T \gamma B^2 \sim 8 \times 10^{18}\ \gamma^{-1}\,[s]$$

$$r_g \sim \gamma m_e c^2 / eB\ , \quad \kappa \sim r_g c / 3\ ,$$
$$v_A \sim B / (4\pi m_p n)^{1/2} \sim 10^8\ cm/s\ ,$$
$$B \sim 10^{-5}\ G\ , \quad R_j \sim 1\ kpc\ .$$

$$t_{esc}/t_{rad} \sim 10^6$$
$$t_{acc} \sim t_{rad} \quad \text{for} \quad \gamma_{eq} \sim 10^8$$

Pile-up synchrotron X-ray emission expected!
(Stawarz & Ostrowski 02, Stawarz+04)

X-ray Jets at High Redshifts

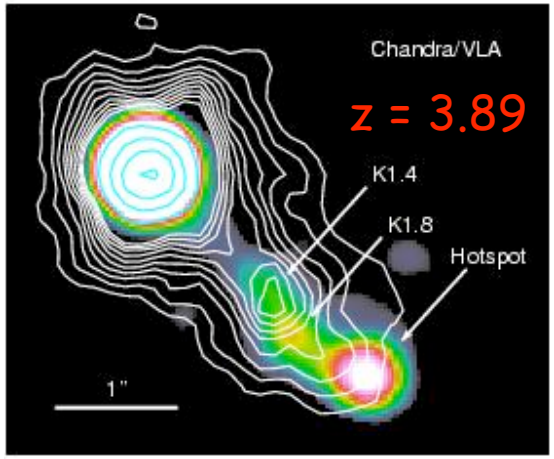

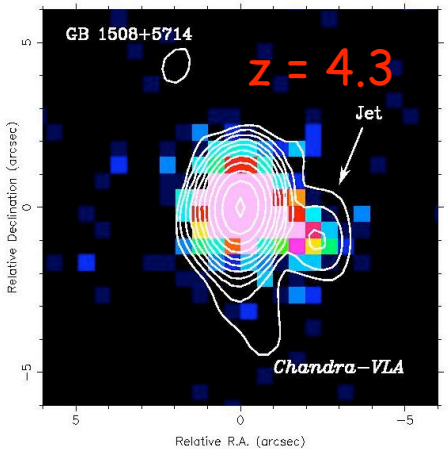

(Siemiginowska+03, Cheung 04, Cheung, Stawarz, Siemiginowska 06, Cheung+09)

$L_{ic/cmb} = (\delta/\Gamma)^2 \times (U'_{cmb}/U'_B) \times L_{syn}$

$U'_{cmb} = 4 \times 10^{-13} (1+z)^4 \Gamma^2$ erg/cm^3

$U_{cmb} \propto (1+z)^4 \Rightarrow$

if the IC/CMB model is correct, then one should expect

- an increase in the X-ray core luminosity with redshift due to unresolved portion of the jet;
- $L_X/L_R \propto (1+z)^4$ for the resolved portion of the jet.

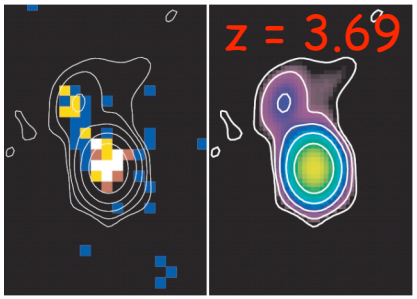

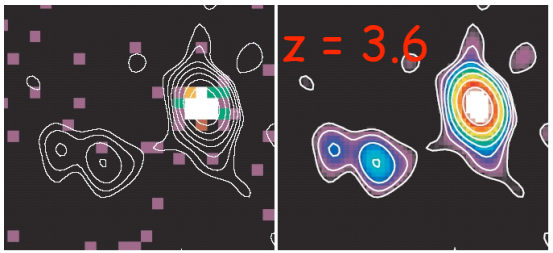

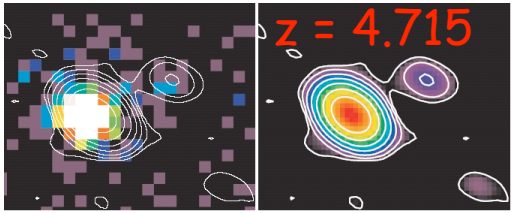

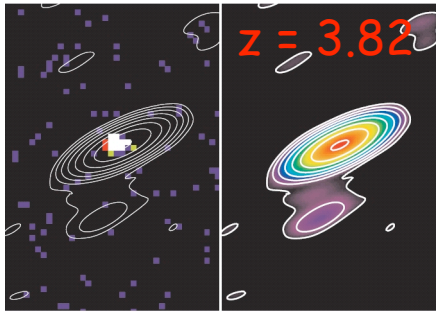

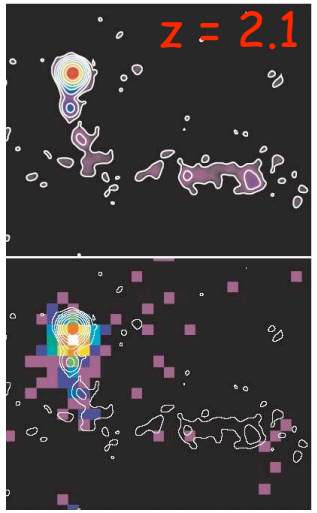

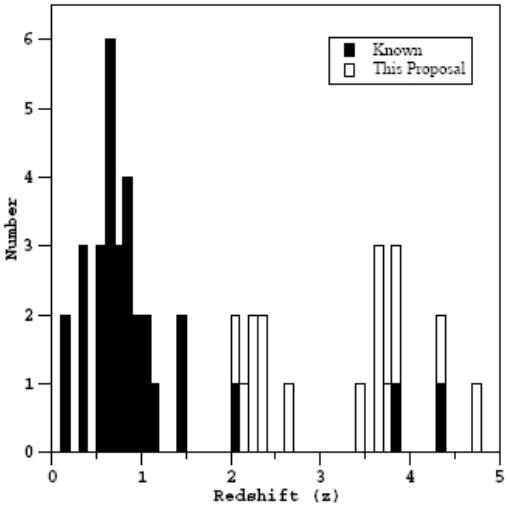

Synchrotron Chandra Jets?

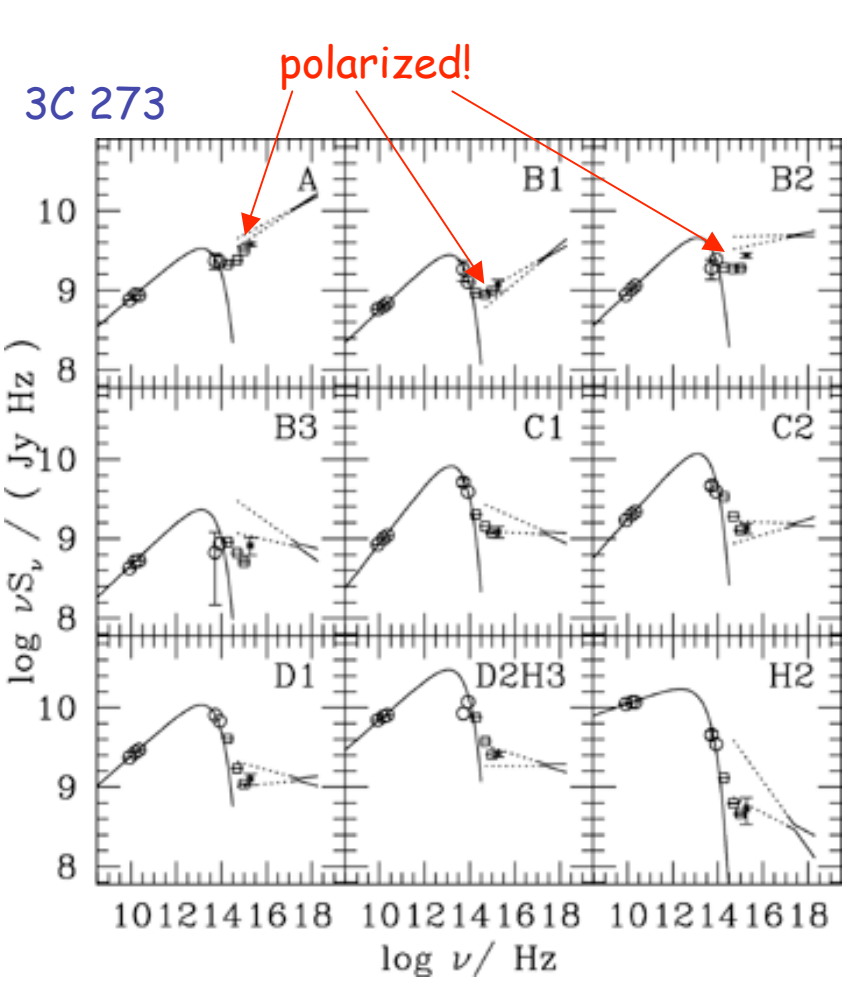

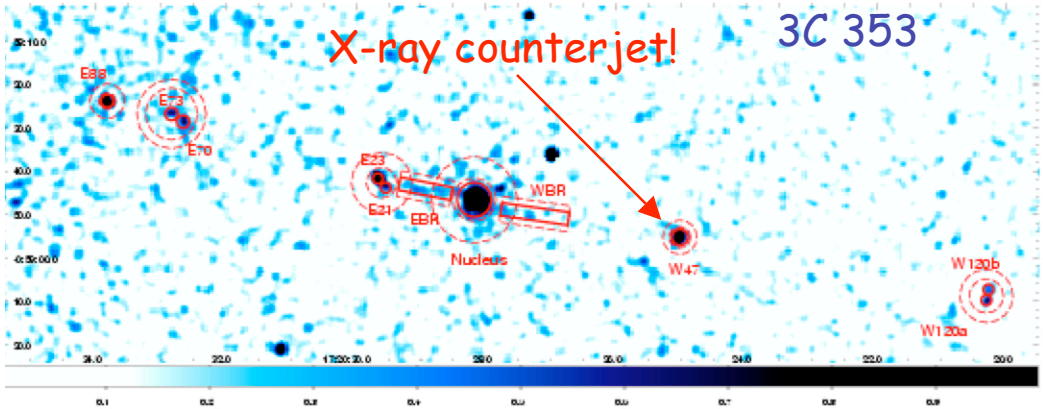

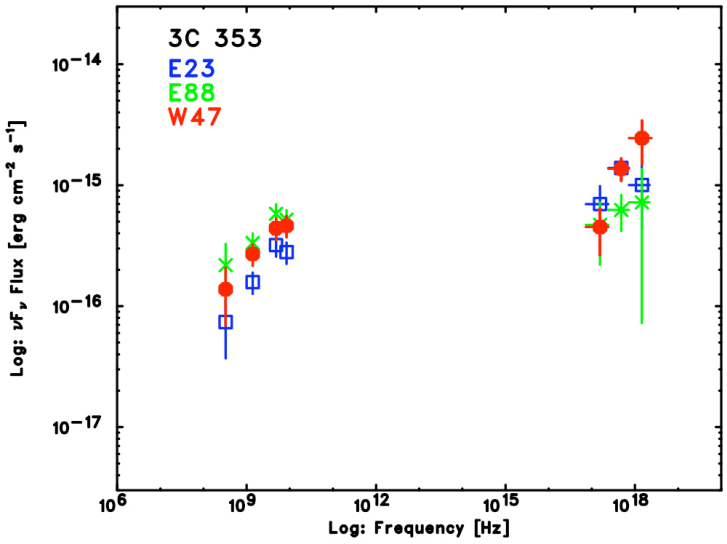

The spectral character of the broad-band emission of 3C 273 jet (**Jester+ 07**), as well as the detection of the X-ray counterjet in FR II radio galaxy 3C 353 (**Kataoka+08**), indicates that the synchrotron scenario for the X-ray emission of Chandra quasar jets may be more likely than the IC/CMB model. In such a case, the jet MF may be as well stronger than or equal to the equipartition value.

Terminal Hotspots

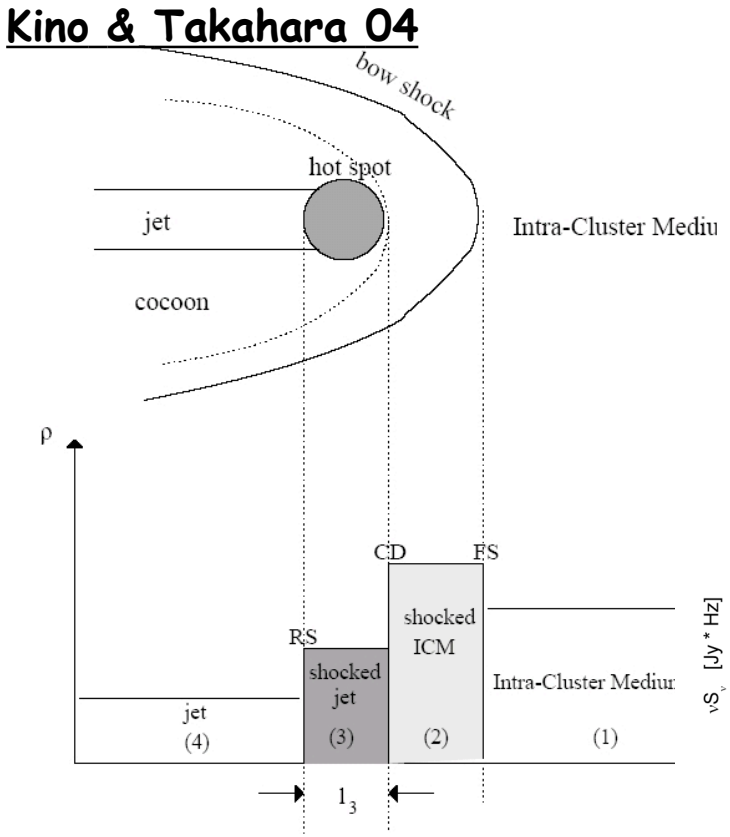

Hotspots in powerful radio sources are understood as the terminal regions of relativistic jets, where bulk kinetic power transported by the outflows from the active centers is converted at a strong shock (formed due to the interaction of the jet with the ambient gaseous medium) to the internal energy of the jet plasma.

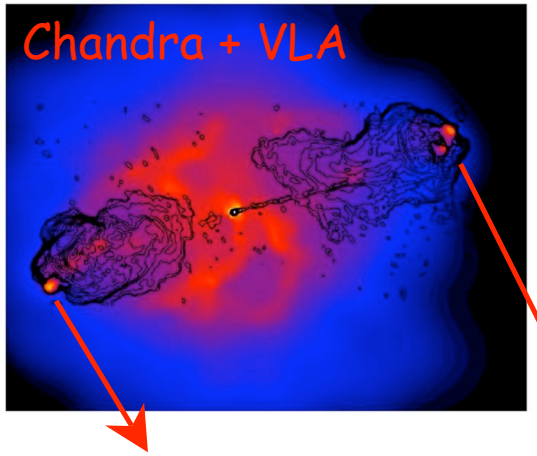

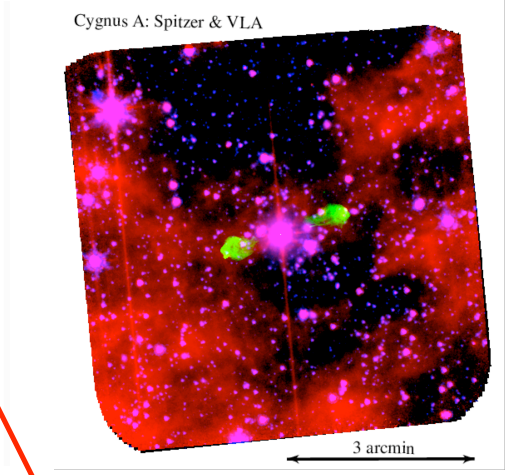

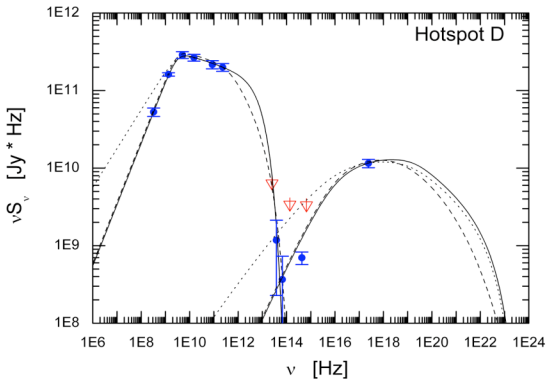

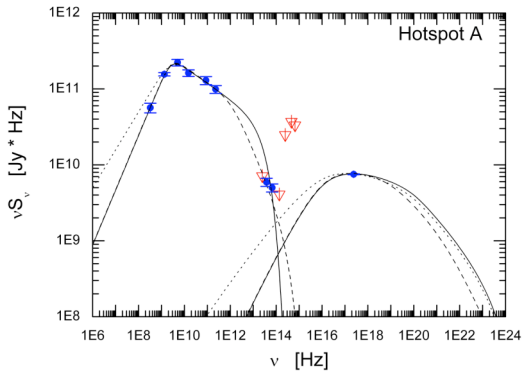

Hotspots of exceptionally bright radio galaxy Cygnus A (d_L = 250 Mpc) can be resolved at different frequencies (VLA, Spitzer, Chandra), enabling us to understand how (mildly) relativistic shocks work (**Stawarz+07**).

Shocks!

Stawarz+07: analysis of the broad-band emission of hotspots in the exceptionally bright radio galaxy Cygnus A indicates $U_B \sim U_e$ and terminal shocks dynamically dominated by protons.

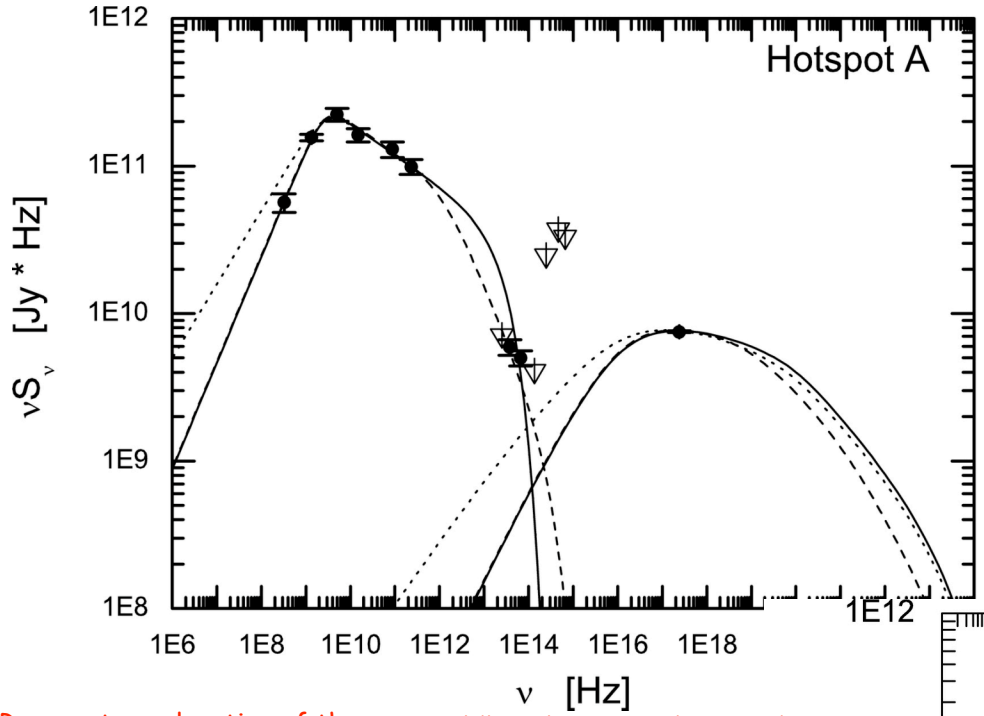

Resonant acceleration of the type discussed by **Hoshino+92** **Amato & Arons 07**

Mildly-relativistic shock with perpendicular MF results in a Steep particle spectrum: **Niemiec & Ostrowski 04**

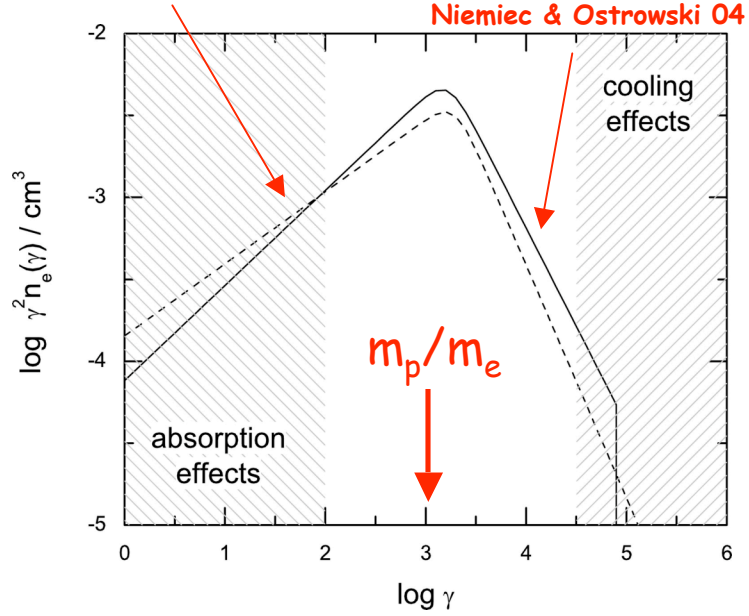

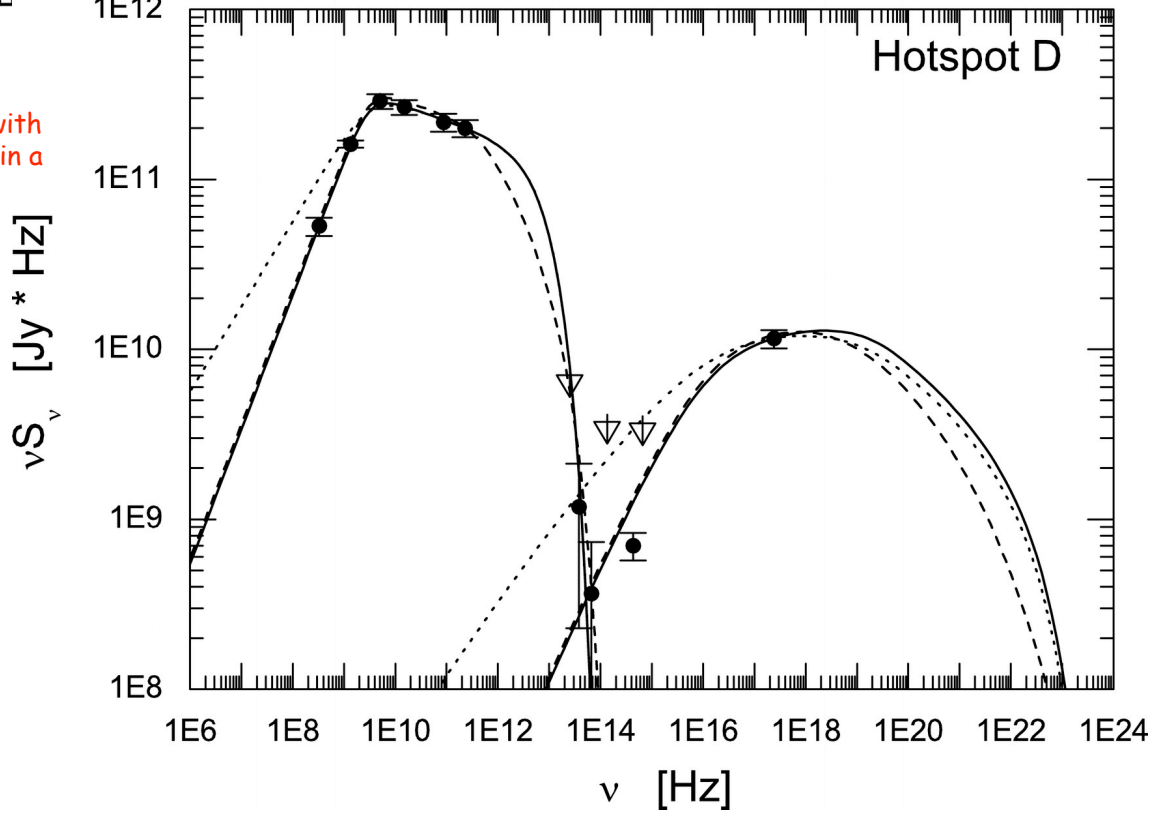

Lobes

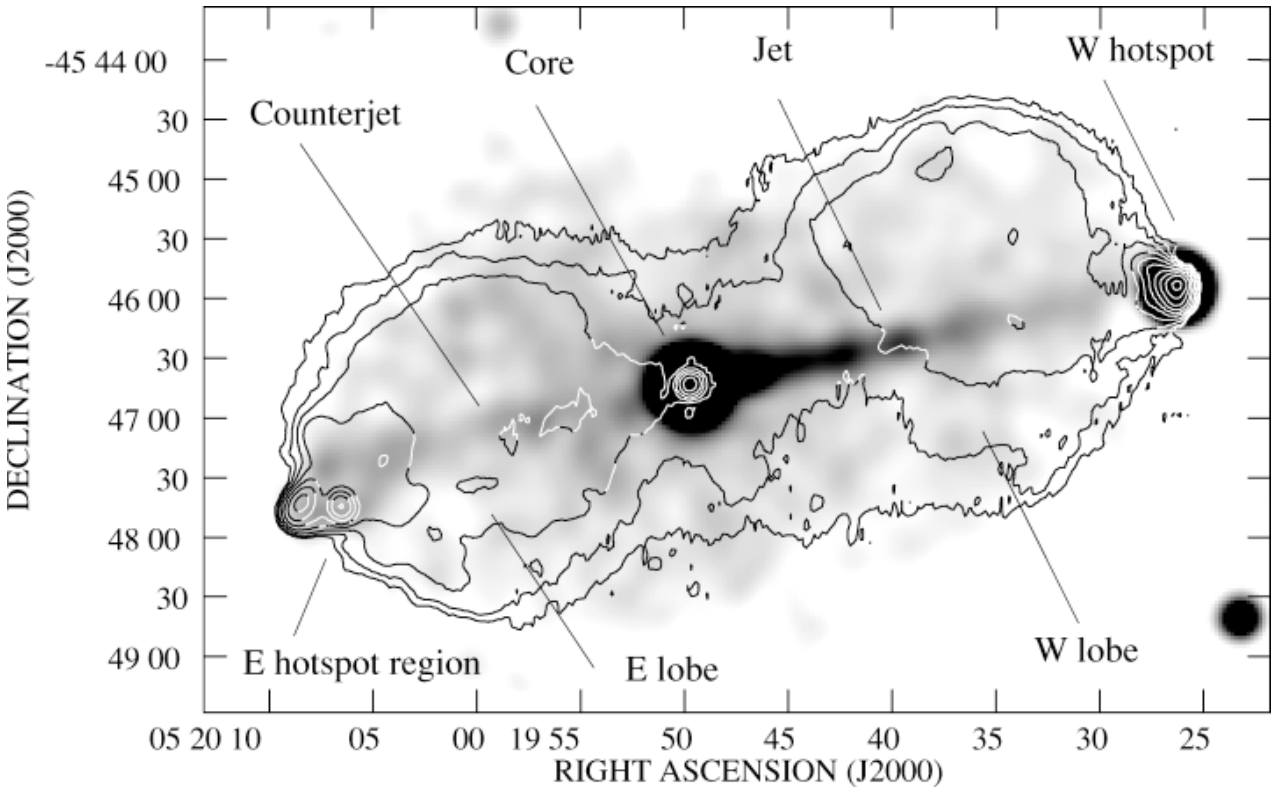

Hardcastle & Croston 05: X-ray and radio emission from the lobes of Pictor A radio galaxy.

X-ray and radio lobe emission in this and many other sources (**Croston+05, Kataoka & Stawarz 05**) indicates energy/pressure equipartition $U_B \sim U_e$.

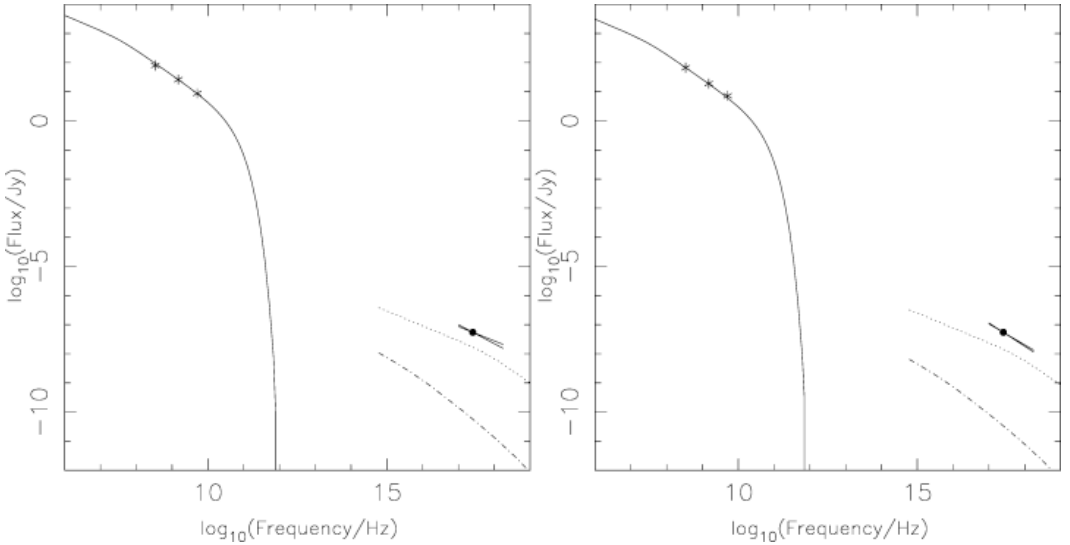

Conclusions

- Magnetic field is crucial in launching AGN jets, since it mediates extraction of the energy and angular momentum from the black hole/accretion disk system.
- Magnetic field is crucial in formation of relativistic jets in AGNs, since it provides collimation and acceleration of nuclear outflows.
- A role of the magnetic field in AGN jets on large scales (confinement, stability, morphology) is still an open question, although most of the observational constraints indicate matter-dominated outflows.
- We do not know exactly how the jet magnetic field mediates energy dissipation (particle acceleration) processes, and therefore how it determines/shapes the high-energy emission of extragalactic jets.